Article

Sub-1.4 cm^3 capsule for detecting labile inflammatory biomarkers in situ

https://doi.org/10.1038/s41586-023-06369-x

Received: 10 May 2022

Accepted: 26 June 2023

Published online: 26 July 2023

Check for updates

M. E. Inda-Webb[1,2,12], M. Jimenez[3,4,5,12], Q. Liu[6], N. V. Phan[4], J. Ahn[4], C. Steiger[3,4,5], A. Wentworth[3,4,5], A. Riaz[6], T. Zirtiloglu[6], K. Wong[5], K. Ishida[3,4,5], N. Fabian[3,4,7], J. Jenkins[3,4], J. Kuosmanen[3,4], W. Madani[3,4,5], R. McNally[5], Y. Lai[1,2], A. Hayward[3,4,5,7], M. Mimee[8], P. Nadeau[9], A. P. Chandrakasan[10], G. Traverso[3,4,5]✉, R. T. Yazicigil[6]✉ & T. K. Lu[1,2,11]✉

Transient molecules in the gastrointestinal tract such as nitric oxide and hydrogen sulfide are key signals and mediators of inflammation. Owing to their highly reactive nature and extremely short lifetime in the body, these molecules are difficult to detect. Here we develop a miniaturized device that integrates genetically engineered probiotic biosensors with a custom-designed photodetector and readout chip to track these molecules in the gastrointestinal tract. Leveraging the molecular specificity of living sensors[1], we genetically encoded bacteria to respond to inflammation-associated molecules by producing luminescence. Low-power electronic readout circuits[2] integrated into the device convert the light emitted by the encapsulated bacteria to a wireless signal. We demonstrate in vivo biosensor monitoring in the gastrointestinal tract of small and large animal models and the integration of all components into a sub-1.4 cm^3 form factor that is compatible with ingestion and capable of supporting wireless communication. With this device, diseases such as inflammatory bowel disease could be diagnosed earlier than is currently possible, and disease progression could be more accurately tracked. The wireless detection of short-lived, disease-associated molecules with our device could also support timely communication between patients and caregivers, as well as remote personalized care.

Our ability to diagnose and monitor inflammatory gastrointestinal disorders would be transformed if we could profile labile, oxidation-related biomarkers and their responses to dietary change and therapies in situ. Many microbiome-related conditions, notably inflammatory bowel disease (IBD), are associated with chronic intestinal inflammation resulting from dysregulated immune homeostasis—specifically, increased oxidation[3,4]. Malnutrition[5], antibiotic resistance[6], antibiotic dysbiosis[7,8], neurodegenerative diseases[9] and mitochondrial genetic disorders[10] are associated with redox imbalance in the gastrointestinal tract, and oxidative stress may also underlie poor responses to chemotherapy[11], and vaccines[12], as well as aging[13].

Bacterial infections[14] and antibiotics[7] may substantially increase concentrations of oxidants, such as reactive oxygen species (ROS) and reactive nitrogen species (RNS). These molecules are labile, which can make it difficult to detect their presence or accurately measure their concentration in the body. Devices reported to sense labile molecules in the gastrointestinal tract (such as oxidizing gases or volatile organic compounds) are limited to off-the-shelf sensors that use non-specific metal-oxide-sensing elements[15,16]. Thus, the current standard of clinical care is limited with respect to our capacity to evaluate the chemical environment underlying the metabolic pathways of both the human host and its resident microorganisms. Developing non-invasive technologies that can continuously monitor the gastrointestinal environment in situ would both expand our understanding of what causes inflammation and indicate directions for improving therapies. Furthermore, diagnosing multi-faceted diseases such as IBD, in which biomarker levels vary substantially among patients, would benefit from the simultaneous detection of a panel of oxidation-related biomarkers (for example, nitric oxide[17] (NO), ROS[18], thiosulfate[19] and tetrathionate[19]).

Current methods of diagnosing gastrointestinal inflammation include endoscopy[20], which is invasive and should only be performed with limited frequency, and stool analysis, which may not accurately reflect intestinal conditions owing to differential growth of certain species[21], ambient oxidation[13] and loss of labile disease-mediating molecules. Culture enrichment[22] (for example, for analysing low-abundance microorganisms in stool samples with omics techniques) may also distort the initial bacterial ratio. Because the faecal microbiota only partially represents the autochthonous microbiota in direct contact with the intestinal mucosa[23], a biopsy may be required for complete analysis[24].

[1]Synthetic Biology Group, MIT Synthetic Biology Center, Department of Biological Engineering, Massachusetts Institute of Technology, Cambridge, MA, USA. [2]Research Laboratory of Electronics, Department of Electrical Engineering and Computer Science, Massachusetts Institute of Technology, Cambridge, MA, USA. [3]Department of Mechanical Engineering, Massachusetts Institute of Technology, Cambridge, MA, USA. [4]The Koch Institute for Integrative Cancer Research, Massachusetts Institute of Technology, Cambridge, MA, USA. [5]Division of Gastroenterology, Brigham and Women's Hospital, Harvard Medical School, Boston, MA, USA. [6]Electrical and Computer Engineering Department, Boston University, Boston, MA, USA. [7]Division of Comparative Medicine, MIT, Cambridge, MA, USA. [8]Department of Microbiology, Biological Sciences Division and Pritzker School of Molecular Engineering, The University of Chicago, Chicago, IL, USA. [9]Analog Devices, Boston, MA, USA. [10]Department of Electrical Engineering and Computer Science, MIT, Cambridge, MA, USA. [11]Senti Biosciences, South San Francisco, CA, USA. [12]These authors contributed equally: M. E. Inda-Webb, M. Jimenez. ✉e-mail: cgt20@mit.edu; rty@bu.edu; timlu@mit.edu

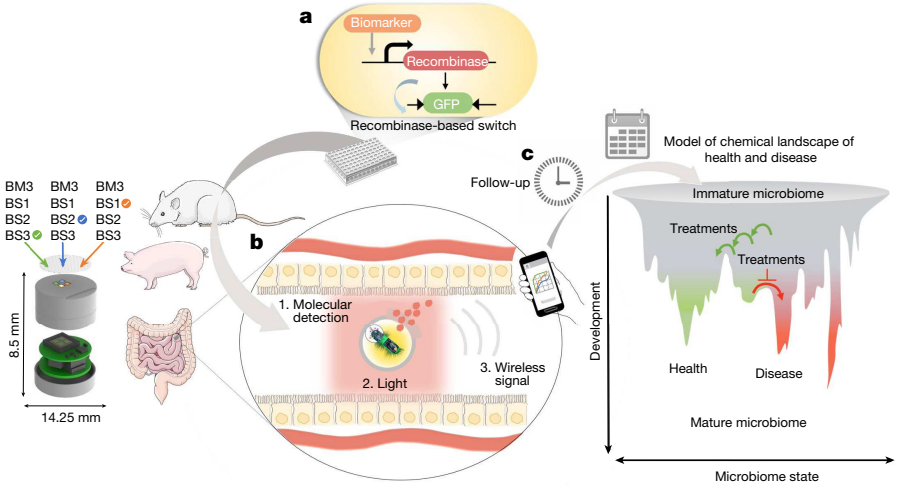

Fig. 1 | General platform for developing a miniaturized capsule for real-time detection of labile mediators of disease in the gut. a, Probiotic bacteria are engineered to respond to an array of IBD biomarkers (BM). A recombinase-based genetic memory system is used to validate the bacterial biosensors (BS) in animal models. Biosensing bacteria are then re-engineered to respond by luminescing and packaged in a capsule that protects the cells during exposure to low pH (such as during passage through the stomach) and interfaces them with miniaturized electronics (the illustration shows the design and dimensions of our fabricated device). **b**, While in transit through the intestines, the biosensing bacteria sense the metabolites as they are being produced inside the body and the miniaturized capsule transmits the bacterial luminescence signal wirelessly to an external device, such as a mobile phone (the wireless signal from the intestinal biomarkers detection has been tested in terminal experiments in pigs). **c**, Top, the device could enable remote detection for immediate follow-up after therapy, as well as monitoring the gut chemical environment for longer-term treatment with personalized therapies or dietary and lifestyle changes. Microbiome dynamics could be characterized as depicted in the simplified model in the bottom right. Starting from infancy, the microbiome gradually reaches one of several adult states characterized by health or disease. Monitoring the gut chemical environment is essential for timely treatments: perturbations that would lead to an unhealthy state can be resisted (red blocked arrow) or an effective treatment plan can be used to return to a healthy state[58] (green arrows). The biosensor image is reproduced from ref. 59.

Engineered living bacteria, due to their innate sensing ability and robust functionality in the gut, have been proposed as a solution to detect analytes associated with intestinal inflammation in complex physiological environments[1]—such as in clinical samples[25] (for example, serum or urine) and inside the gut, detecting either biomolecules supplemented in diet[26–28] or by-products of inflammation[19,29,30]. However, current applications of biosensors still depend on the complex analysis of bacterial gene expression, RNA or DNA in stool, rather than real-time reporting from localized regions within the body.

Electronic devices that continuously collect, process and wirelessly transmit information can also be used to analyse the gastrointestinal tract. However, capsule endoscopy cameras currently approved by the US Food and Drug Administration[31] do not directly measure the molecular mediators of disease such as ROS or RNS. Other ingestible, ultralow-power electronic devices currently under development can be used to visually evaluate the gastrointestinal tract and measure gas concentrations, temperature and pH levels[15,32] but require functionalization with fragile transducers to convert biochemical information into electronic signals, which limits specificity and robustness[15,33].

To overcome these challenges and to leverage the promise of transient biomarker panels, we combined natural protein-based sensing elements for NO, hydrogen peroxide (H_2O_2), tetrathionate and thiosulfate with genetically encoded memory circuits, incorporated them into probiotic bacteria, and validated their function in vivo in mouse and pig models of inflammation. We then integrated these bacterial sensors with a custom-designed integrated photodiode array and readout chip. This integrated system builds on our early prototype[34], which was only validated for the detection of blood in vivo but was considerably larger (more than 9 cm^3) than any known safe ingestibles. The new pill has a volume of less than 1.4 cm^3 and a pill form factor that conforms to the size of safe ingestible non-deformable dosage forms on the market[35]. Our miniaturized wireless bio-electronic pill can safely process data with low power consumption and transmit it to a portable device such as a smartphone. We have tested this multi-diagnostic pill in live pigs, demonstrating that a human-scale diagnostic device can be built to detect transient mediators of gastrointestinal inflammatory diseases (Fig. 1).

Design of biosensing genetic circuits

Intestinal bacteria have natural sensors that continuously detect specific molecules in the gut. We chose probiotic *Escherichia coli* Nissle 1917 as a chassis owing to its resilience and excellent safety profile in the gastrointestinal tract[36], and engineered it to detect the labile IBD-mediating molecules NO, H_2O_2, thiosulfate and tetrathionate (Extended Data Fig. 1).

We first optimized the NO sensor by combining the bacterial NO biosensor NorR[17,37,38] with a DNA recombinase core circuit[39] to create memory circuits that could record NO exposure of bacterial biosensors as they travelled through the gastrointestinal tract (Fig. 2a) in the dextran sodium sulfate (DSS) model of intestinal inflammation in mice. Because the recorded information is stored in the DNA and passed from generation to generation, it can be retrieved by measuring GFP expression from the bacteria recovered from faeces. Using flow cytometry, the percentage of cells that were GFP 'ON'[18] (the percentage of GFP-positive cells) was calculated at each concentration of diethylenetriamine–nitric oxide adduct (DETA–NO). After multiple rounds of optimization to improve the signal-to-noise ratio (SNR) of the genetic circuits and characterization (Extended Data Fig. 2a–c), our NO recombinase-based memory system responded to a concentration threshold of 30 μM NO with high specificity and was not influenced by other RNS (NOx) present in the gut environment (Fig. 2a). The NO sensor was tested under anaerobic conditions (Extended Data Fig. 2d) and over time (Extended Data Fig. 2e,f). Similarly, we built recombinase-based memory circuits to optimize the detection of H_2O_2, thiosulfate and tetrathionate (Extended Data Fig. 3a–d).

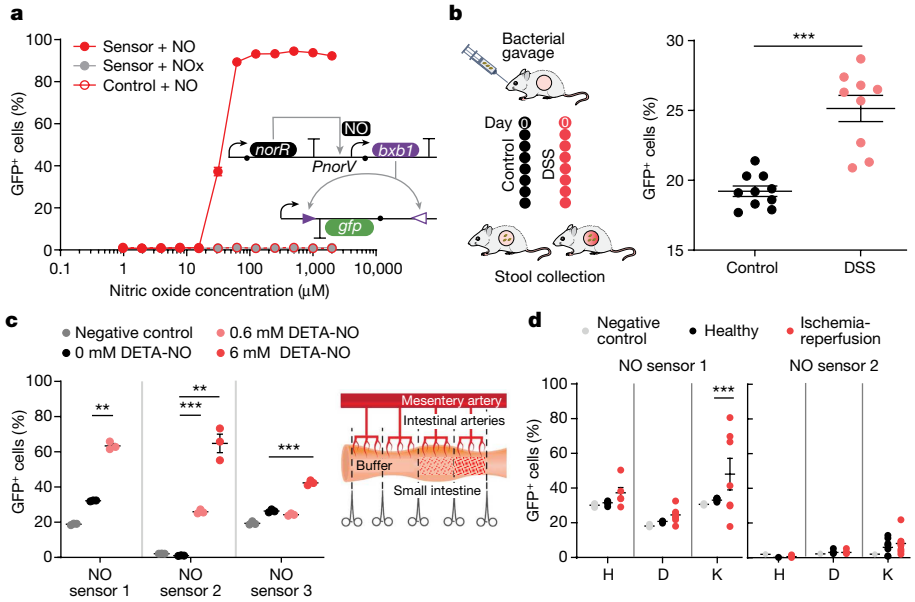

Fig. 2 | Validation in vitro and in vivo of probiotic bacteria engineered to detect NO. a, Inset, in response to NO, the transcription factor NorR binds to the PnorV promoter (inset), activating the transcription of bxb1 recombinase, leading to inversion of the *gfp* expression cassette (located between attB and attP sites, triangles) and expression of GFP. Flow cytometry was used to determine the percentage of GFP-positive cells at various NO concentrations. RNS other than NO (NOx) did not activate the system. $n = 3$ per group. **b**, Left, experimental timeline for validation in mice. C57BL/6 male mice were treated for 7 days with 3% DSS in drinking water. DSS-treated mice and control were gavaged every other day with engineered bacteria carrying the NO memory system. Stool was collected 6 h after gavage. Right, the NO sensor was significantly activated on day six of DSS treatment. DSS: $n = 10$; control: $n = 10$. Sensor 1: $^{**}P = 0.0015$; sensor 2: $^{**}P = 0.0067$, $^{***}P = 0.0007$; sensor 3: $^{***}P = 0.002$. Two-tailed unpaired Student's *t*-test. **c**, The NO sensor was validated in pigs. Right, experimental design: intestines were clamped to separate control and treated compartments. Bacterial NO sensors 1, 2 and 3—with activation thresholds of 0.6 mM, 0.6 to 6 mM and 6 mM DETA–NO, respectively—were placed in the different compartments. $n = 3$ per group. **d**, Ischaemia-reperfusion model of inflammation in pigs. Data are shown from four independent experiments (four pigs: H, D, M and K) on different days, with multiple compartments per animal. $^{***}P = 0.0005$. Two-way ANOVA for multiple comparisons. In **c**,**d**, bacteria were collected from the intestine after two hours of exposure to the analyte or the ischaemia-reperfusion. In **b**–**d**, the percentage of GFP-positive cells was measured by flow cytometry ($n = 10{,}000$ events) from separately grown culture after retrieval. Data are mean ± s.e.m.

We also created a disease-stage detector based on the concentration of NO detected, which would indicate whether inflammation was mild, moderate or severe (Extended Data Fig. 3e). The incorporated recombinase-based switch was also used to discretize the biomarker input levels and create digital memories in the cells[18]. Tuning the sensitivity of the NO biosensor resulted in different activation thresholds, so that physiologically relevant concentrations of the biomarker (low, medium or high) could be measured in animal models. All of the sensors developed for in vivo validation in mice measured GFP expression as a readout of the memory system activation; the sensors were activated within minutes (Extended Data Fig. 2e), making them suitable for detection in the intestine[36].

Biosensors detect disease in animal models of IBD

To examine the in vivo functionality of our bacterial sensors, we evaluated whether they could detect chemically induced gastrointestinal inflammation while passing through the gastrointestinal tract in a mouse model of colitis (Fig. 2b). After inflammation was induced with DSS, control and treated mice were orally gavaged with the NO biosensors. Six hours later[34], the percentage of GFP^+ cells recovered from faecal samples was analysed by flow cytometry. NO biosensors detected significantly more GFP^+ cell activation in faecal pellets from treated mice than in those from healthy controls (Fig. 2b). Inflammation in the colitis model was measured over time (Extended Data Fig. 4a) and independently validated (Extended Data Fig. 4b,c). Our biosensor thus detected the presence of NO as a marker of gastrointestinal inflammation in vivo.

GFP activation increased significantly at day nine after the start of DSS treatment (Extended Data Fig. 4a), correlating with the peak of inducible nitric oxide synthase (iNOS) activation[40]. Tracking NO with the disease-stage detector revealed an exacerbated inflammatory response following antibiotic treatment in a chronic inflammation model (Extended Data Fig. 4d,e). We also tested our bacterial sensors for detection of ROS (H_2O_2), tetrathionate and thiosulfate; activation was detected as inflammation progressed, with thiosulfate detection at day six after the start of DSS treatment and tetrathionate (a product of thiosulfate oxidation) detection at day ten, overlapping with ROS detection (Extended Data Fig. 3b,c).

To validate the bacterial sensors in a disease model that is similar in physiology and scale to human anatomy[41], we tested the bacterial biosensors in living pigs using an ischaemia-reperfusion injury model of intestinal inflammation[42]. We injected the bacterial biosensors directly into the intestinal lumen of a sedated pig, in either inflamed segments or healthy segments with or without added biomarkers. The NO-sensing bacteria detected different concentrations of NO in the control group (Fig. 2c) and emitted a positive signal in some of the animals in the disease group (ischaemia-reperfusion; Fig. 2d). Although previous direct NO measurements in inflamed intestines are limited and uncertain, based on the lowest detectable signal from the NO biosensor bacteria 1 (around 8 μM; Extended Data Fig. 3e) our results agree with an estimated range of expected NO (1–10 μM) in humans and suggest that the biosensors are functional in the complex, dynamic environment of an inflamed intestine[43]. Additionally, the ROS, thiosulfate and tetrathionate sensors also detected significant quantities of analytes in control-treated pigs (Extended Data Fig. 4f).

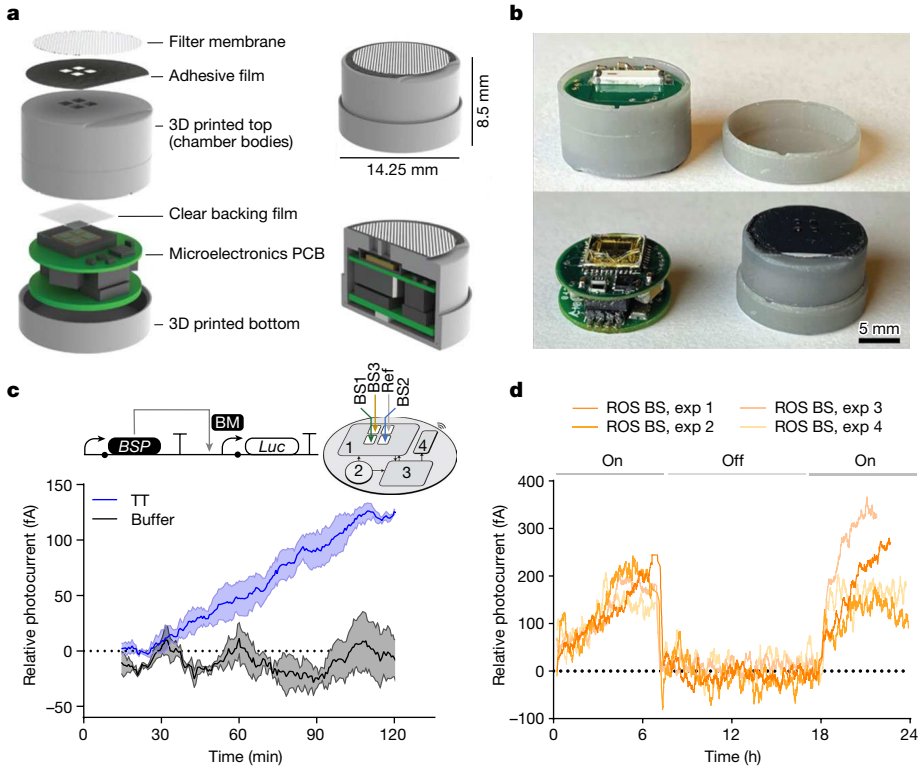

Fig. 3 | Design and in vitro characterization of a device for miniaturized wireless sensing with cell-based biosensors. a, Components and dimensions of the device. **b**, Design of a miniaturized pill casing with a bacterial-electronic chamber interface. Top, side view of the device. Bottom, fully assembled pill with the permeable membrane attached. The bacterial chamber–casing unibody design uses a thin clear backing film to place the bacteria close to the photosensitive electronic chip. A double-sided adhesive film enables a low-profile seal to the permeable outer filter membrane. **c**, Top left, the genetic circuit and wireless signal over time from the tetrathionate sensor encapsulated in the device and immersed in bacterial growth media supplemented with 100 mM tetrathionate. Low-power CMOS-integrated photodiodes convert bioluminescence emitted from the bacterial sensor to a photocurrent, which is converted to quantifiable digital data and transmitted wirelessly to the external device. Top right, Multiple biosensors (BS) can be used together with this array to study a metabolic pathway (for example, H_2O_2, thiosulfate and tetrathionate sensors; Extended Data Fig. 3c). (1) A threshold-based bioluminescence detector with a CMOS-integrated photodiode[2] array was used to detect bacterial sensor output; (2) battery; (3) microcontroller and radio chip; (4) antenna. Lines represent the mean and the shaded area indicates the the s.e.m. for three independent replicates, conducted with one induced device (tetrathionate) and one uninduced device (buffer). BM, biomolecule that induces the circuit; BSP, biosensing protein; *Luc*, luciferase reporter operon; ref, reference chamber. **d**, In vitro characterization of the device for long-term use, measuring reversibility over time for 24 h. Probiotic bacteria engineered to detect ROS (ROS BS) were encapsulated in the device and immersed in bacterial growth media intermittently supplemented with 20 mM H_2O_2 to test reversibility. Wireless signals were recorded over time. The dynamic circuit for ROS performed with stringent control during the off phase and showed a perfect reactivation over the second on phase. Lines represent four independent replicates (exp 1–4) conducted with two different chips on different days over multiple cycles induced with 20 mM H_2O_2, followed by a wash and incubation in growth medium and induced again by supplementing the growth medium with 20 mM H_2O_2.

Validation of a bacterial-electronic sensor pill

To advance our bacterial sensors towards clinical application, we integrated them into a bacterial-electronic pill. Specifically, we designed a system with a size and form factor conforming to a proven non-deformable dosage form (Extended Data Fig. 5a) by developing an optimized luminescent readout via a custom microelectronic bioluminescence detector[2] and bacterial chambers built directly into the pill casing.

Our multi-diagnostic device requires nutrients and analytes to be exchanged efficiently while retaining the engineered microorganisms and simultaneously allowing the generated light signal to reach the electronic detectors. Thus, we developed a pill casing that incorporates a bacterial-electronic chamber interface in a unibody design (Fig. 3a,b) in which the bacteria are precisely aligned in a tablet-shaped two-by-two array with the microelectronic photodiodes and a hermetic seal is maintained around the electronic components. This design enabled sensing from an array of engineered microbial strains expressing luciferase in response to several biomarkers (NO, ROS, tetrathionate and negative reference). To retain the bacterial cells, the integrated chambers (Extended Data Fig. 5b) were sealed with porous membranes (nominal pore size, 0.4 µm), which did not interfere with the detection of the target molecules when the chambers were placed in faeces (Extended Data Fig. 6a). Additionally, to protect the on-board bacteria during ingestion and transit through the stomach, we developed free-standing enteric polymer films that prevent low pH ingress through simulated ingestion (Extended Data Figs. 6b–e and 7). To generate versions of the bacterial sensors that can optimally couple to the photosensitive electronics, we replaced the GFP readout with a self-contained bioluminescence readout, the luxCDABE operon from *Photorhabdus luminescens*[34], and the memory system with a reversible analogue output. We constructed this genetic circuit in *E. coli* Nissle 1917 and exposed the resultant strain to DETA–NO as a source of NO (Extended Data Fig. 8a–c). The NO-biosensing bacteria responded rapidly to DETA–NO exposure (time to reach maximum signal (t_{max}) = 60 min) with a high luminescence output and a SNR of 170 (Extended Data Fig. 8a). Production of the luminescence machinery was also induced by DETA–NO in cultures grown under anaerobic conditions (Extended Data Fig. 8d) and the machinery was stable through simulated ingestion (Extended Data Fig. 7). ROS, thiosulfate and tetrathionate sensors were also built in combination with

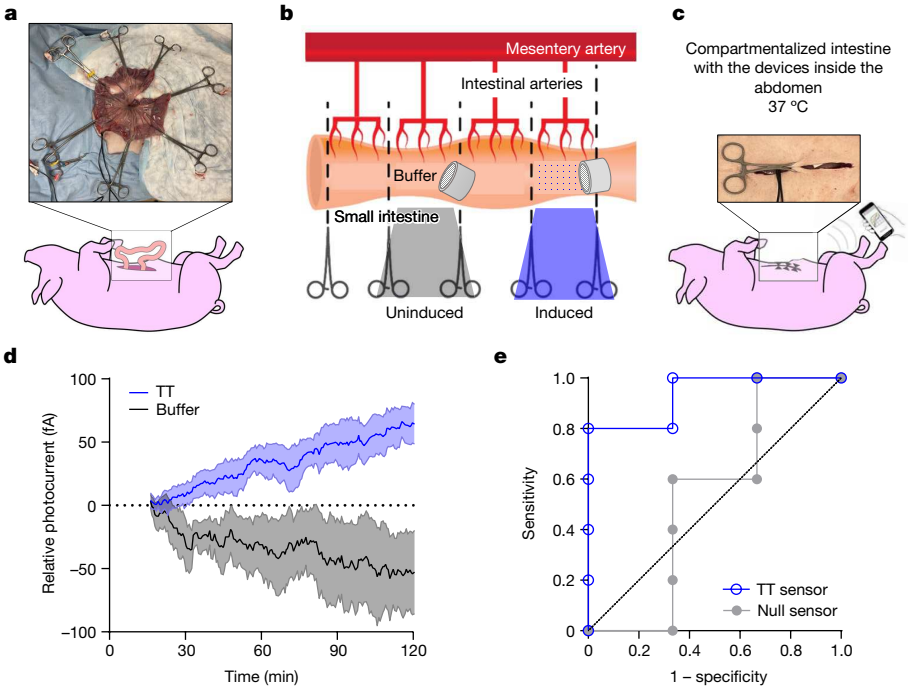

Fig. 4 | Validation of the integrated device for miniaturized wireless biosensing in live pigs. a, Schematic of the experiment. The bacterial biosensors encapsulated in the device were tested in situ in a terminal procedure in anaesthetized Yorkshire pigs weighing around 90 kg. After opening the abdominal cavity, we placed the device through a small incision directly into the lumen of the small intestine, compartmentalized with clamps. **b**, Schematic of compartmentalization of a section of the intestine that was clamped for experimentation. Tetrathionate (100 mM) was injected with a syringe into the clamped intestinal compartment. Buffer was added as a control in a different compartment. **c**, Compartmentalized intestines were kept inside the abdomen at 37 °C. Wireless signals transmitted from inside the abdomen were detected by a commercial receiver, which can be connected to a laptop computer or a mobile phone. **d**, Kinetics of the tetrathionate sensor embedded in the abdominal cavity of a pig. The response of the device placed in the compartment with tetrathionate was clearly distinguishable from that of the device in the compartment with the buffer control. Dark lines represent the mean of independent experiments in different pigs with up to two devices in separate compartments (tetrathionate (TT) and buffer) and the shaded area represents the s.e.m. Tetrathionate: $n = 5$; buffer: $n = 3$. **e**, The receiver operating characteristic of the device with sensing after 60 min.

the luxCDABE operon for real-time detection and characterized in vitro (Fig. 3c and Extended Data Fig. 8a–c); the tetrathionate sensor reached the highest luminescence values in simulated intestinal fluid (Extended Data Fig. 8b) and was selected for initial optimization of an integrated device. Finally, we designed a millimetre-scale capsule printed circuit board (PCB) housing a complementary metal-oxide-semiconductor (CMOS) bioluminescence detector chip with an integrated photodiode array achieving high sensitivity (Fig. 3c). The custom chip integrates a threshold-based bioluminescence detector, time-to-digital converter, voltage references, voltage regulators and four 1 mm × 1 mm CMOS-compatible photodiodes[2] (Extended Data Fig. 9a). Besides the custom chip, the miniaturized capsule includes a commercial microcontroller and wireless transmitter. Bioluminescence from activated cells was detected by CMOS-integrated photodiodes located below each chamber. Custom-designed electronics processed the luminescence data by periodically sampling the photon-generated charge (with a programmable integration time of approximately 26 s). The detected luminescence was converted to a digital code by the low-power luminescence readout chip and transmitted wirelessly for calibration, display and recording.

In vitro, with 1 µl of sensor bacteria culture per chamber, the integrated device detected the presence of tetrathionate. We recorded 125 fA of relative photocurrent produced by the induced tetrathionate bacteria sensor, with a baseline of around 0 fA from the uninduced control (Fig. 3c). We next evaluated the performance of the other bacterial sensors in this optimized, integrated electronic pill. Although the thiosulfate sensor did not have a luminescence readout compatible with the electronics (as expected from the plate reader-based characterization in Extended Data Fig. 8c), the NO and ROS sensors could successfully interface with the pill to give an electronic readout in the presence of the target molecules (Extended Data Fig. 9b,c) and even show reversibility (Fig. 3d; ROS sensor).

To model the complex milieu of the gastrointestinal tract, the integrated device was also tested in vivo in pig small intestines. Upon induction, luminescence was detected by the custom-designed electronic readout circuits in the capsule; the information was wirelessly transmitted in real time from inside the body of the living pig to an external recording device (Fig. 4a–c). This design enabled remote monitoring of biomolecules in the gut for 4 h, with 70 fA relative photocurrent detected in the induced compartment, and a baseline of −50 fA from the uninduced control (Fig. 4c and Extended Data Fig. 10a–c). The receiver operating characteristic of the tetrathionate sensing showed a detection latency of 1 h and reached a sensitivity and specificity of 100% at 120 min; thus, the miniaturized device can effectively detect the target analyte in the harsh intestinal environment (Fig. 4d and Extended Data Fig. 10d).

Discussion

We have built a microbial biosensor that is compatible with ingestion and can sense an array of biomarkers in situ as they are being produced. This technology can potentially support remote disease management by providing quantitative, real-time and multiplexed information linking perturbations in the gastrointestinal tract microbiome to disease. To validate the cell-based biosensors in preclinical disease models, we coupled engineered sensing bacteria with a recombinase-based memory system. Our memory system records information as soon as metabolites are produced in the gut, activating switches within minutes

of exposure. The recombinase-based switch discretizes the magnitude of a given biomarker; this quantitative response may align with disease stage and therefore indicate the severity of inflammation. Although the parameters measurable with this device may have no absolute 'healthy' range, measurements taken over time may reveal patterns predictive of acute disease episodes (flares), making it possible to anticipate disease symptoms. Similarly, the switch acts as a peak detector for sensing and recording maximum levels of intestinal biomarkers.

To create our miniaturized low-power electronic device, we integrated CMOS-compatible photodiodes with discrete-time signal processing circuits. The whole capsule, which is less than 1.4 cm^3 in size, can simultaneously detect multiple disease biomarkers on a stringent power budget. With the integrated CMOS system and pill casing design, we could detect the bioluminescent signal from just 1 µl of bacterial culture in the milieu of the intestinal lumen. Furthermore, a coin-cell battery can power the miniaturized capsule for a month[2], so this device could also potentially be used as an implant[44,45].

We also demonstrated that the use of solid, non-deformable devices and free-standing polymer films provides a means to protect both the viability and the function of the on-board biosensor bacteria through the harsh environment of the stomach. Beyond this initial line of defence, the filter membrane also serves to contain the biosensor cells while excluding host immune and microbial cells, preventing unexpected off-target interactions and enhancing biocontainment while allowing free exchange of nutrients and other small molecules of interest for sensing[46,47]. Our device-based protection strategy is also orthogonal to and can be combined with direct cell encapsulation strategies based on secretion of capsular polysaccharides[48], hydrogels[44] and synthetic coating of microbial surfaces (alginate[49], chitosan[49], polydopamine[50], lipids[51] and nanoparticles[52]) that can provide downstream protection against bile acids, antimicrobials and bacteriophages.

The diagnostic accuracy and specificity of our device are based on the simultaneous testing of multiple labile by-products of inflammation (such as NO and ROS), intestinal gases (such as H_2S, measured as thiosulfate) and other important molecules for the microbiome (for example, tetrathionate). As biomarker levels may vary greatly among individuals, a panel of biomarkers would be required to accurately diagnose IBD and other multi-faceted diseases.

Our miniaturized device offers a route for non-invasively evaluating changes in the intestinal biochemical milieu and overcomes the limitations of microbiome characterization by 16S rRNA or metagenomic sequencing[53,54], as well as those of existing ingestible biosensors used in animal models, which require the complex analysis of microbial gene expression, RNA or DNA in stool[19,26–29]. The biosensors described here also have the potential to expand the range of biomarkers being targeted by other ingestible electronic systems[55]. The capsule could be designed to report its location while in transit[56] and perform cell-based computation to further expand the multiplex capabilities of the underlying electronic system. For example, AND gates[57] could be incorporated to determine the co-localization of biomarkers for understanding metabolic pathways or biomarker discovery in animal models for many microbiome-linked diseases.

We envision that with further clinical testing in humans, this device could be developed as a first-line at-home screen for non-invasive continuous monitoring of the chemical environment of the gastrointestinal tract and customized for numerous gastrointestinal disorders, with the potential to be a safer and inexpensive point-of-care alternative to endoscopy. Tracking and quantitatively assessing multiple biomarkers would provide a potential framework for patients to assess the effects of diet, lifestyle and other interventions to improve health outcomes.

Online content

Any methods, additional references, Nature Portfolio reporting summaries, source data, extended data, supplementary information, acknowledgements, peer review information; details of author contributions and competing interests; and statements of data and code availability are available at https://doi.org/10.1038/s41586-023-06369-x.

1. Inda, M. E. & Lu, T. K. Microbes as biosensors. *Annu. Rev. Microbiol.* **74**, 337–359 (2020).
2. Liu, Q. et al. A threshold-based bioluminescence detector with a CMOS-integrated photodiode array in 65 nm for a multi-diagnostic ingestible capsule. *IEEE J. Solid State Circuits* **58**, 838–851 (2023).
3. Bourgonje, A. R. et al. Oxidative stress and redox-modulating therapeutics in inflammatory bowel disease. *Trends Mol. Med.* **26**, 1034–1046 (2020).
4. Lee, J.-Y., Tsolis, R. M. & Bäumler, A. J. The microbiome and gut homeostasis. *Science* **377**, eabp9960 (2022).
5. Million, M. et al. Increased gut redox and depletion of anaerobic and methanogenic prokaryotes in severe acute malnutrition. *Sci. Rep.* **6**, 26051 (2016).
6. Pribis, J. P. et al. Gamblers: an antibiotic-induced evolvable cell subpopulation differentiated by reactive-oxygen-induced general stress response. *Mol. Cell* **74**, 785–800.e7 (2019).
7. Reese, A. T. et al. Antibiotic-induced changes in the microbiota disrupt redox dynamics in the gut. *eLife* **7**, e35987 (2018).
8. Rivera-Chávez, F. et al. Depletion of butyrate-producing clostridia from the gut microbiota drives an aerobic luminal expansion of *Salmonella*. *Cell Host Microbe* **19**, 443–454 (2016).
9. Dumitrescu, L. et al. Oxidative stress and the microbiota–gut–brain axis. *Oxid. Med. Cell. Longev.* **2018**, 2406594 (2018).
10. Yardeni, T. et al. Host mitochondria influence gut microbiome diversity: A role for ROS. *Sci. Signal.* **12**, eaaw3159 (2019).
11. Jose, S., Bhalla, P. & Suraishkumar, G. K. Oxidative stress decreases the redox ratio and folate content in the gut microbe, *Enterococcus durans* (MTCC 3031). *Sci. Rep.* **8**, 12138 (2018).
12. Hagan, T. et al. Antibiotics-driven gut microbiome perturbation alters immunity to vaccines in humans. *Cell* **178**, 1313–1328.e13 (2019).
13. Million, M. & Raoult, D. Linking gut redox to human microbiome. *Hum. Microbiome J.* **10**, 27–32 (2018).
14. Rivera-Chávez, F. & Bäumler, A. J. The pyromaniac inside you: *Salmonella* metabolism in the host gut. *Annu. Rev. Microbiol.* **69**, 31–48 (2015).
15. Kalantar-Zadeh, K. et al. A human pilot trial of ingestible electronic capsules capable of sensing different gases in the gut. *Nat. Electron.* **1**, 79–87 (2018).
16. Steiger, C. et al. Dynamic monitoring of systemic biomarkers with gastric sensors. *Adv. Sci.* **8**, 2102861 (2021).
17. Archer, E. J., Robinson, A. B. & Süel, G. M. Engineered *E. coli* that detect and respond to gut inflammation through nitric oxide sensing. *ACS Synth. Biol.* **1**, 451–457 (2012).
18. Rubens, J. R., Selvaggio, G. & Lu, T. K. Synthetic mixed-signal computation in living cells. *Nat. Commun.* **7**, 11658 (2016).
19. Daeffler, K. N. et al. Engineering bacterial thiosulfate and tetrathionate sensors for detecting gut inflammation. *Mol. Syst. Biol.* **13**, 923 (2017).
20. Annese, V. et al. European evidence-based consensus: inflammatory bowel disease and malignancies. *J. Crohns. Colitis* **9**, 945–965 (2015).
21. Amir, A. et al. Room-temperature, correcting for microbial blooms in fecal samples during shipping. *mSystems* **2**, e00199–16 (2017).
22. Raymond, F. et al. Culture-enriched human gut microbiomes reveal core and accessory resistance genes. *Microbiome* **7**, 56 (2019).
23. Zmora, N. et al. Personalized gut mucosal colonization resistance to empiric probiotics is associated with unique host and microbiome features. *Cell* **174**, 1388–1405.e21 (2018).
24. Jain, U. et al. *Debaryomyces* is enriched in Crohn's disease intestinal tissue and impairs healing in mice. *Science* **371**, 1154–1159 (2021).
25. Courbet, A., Endy, D., Renard, E., Molina, F. & Bonnet, J. Detection of pathological biomarkers in human clinical samples via amplifying genetic switches and logic gates. *Sci. Transl. Med.* **7**, 289ra83 (2015).
26. Kotula, J. W. et al. Programmable bacteria detect and record an environmental signal in the mammalian gut. *Proc. Natl Acad. Sci. USA* **111**, 4838–4843 (2014).
27. Lim, B., Zimmermann, M., Barry, N. A. & Goodman, A. L. Engineered regulatory systems modulate gene expression of human commensals in the gut. *Cell* **169**, 547–558.e15 (2017).
28. Mimee, M., Tucker, A. C., Voigt, C. A. & Lu, T. K. Programming a human commensal bacterium, *Bacteroides thetaiotaomicron*, to sense and respond to stimuli in the murine gut microbiota. *Cell Syst.* **1**, 62–71 (2015).
29. Riglar, D. T. et al. Engineered bacteria can function in the mammalian gut long-term as live diagnostics of inflammation. *Nat. Biotechnol.* **35**, 653–658 (2017).
30. Pickard, J. M. et al. Rapid fucosylation of intestinal epithelium sustains host–commensal symbiosis in sickness. *Nature* **514**, 638–641 (2014).
31. Swain, P. Wireless capsule endoscopy. *Gut* **52 (suppl. 4)**, 48–50 (2003).
32. van der Schaar, P. J. et al. A novel ingestible electronic drug delivery and monitoring device. *Gastrointest. Endosc.* **78**, 520–528 (2013).
33. Din, M. O. et al. Interfacing gene circuits with microelectronics through engineered population dynamics. *Sci. Adv.* **6**, eaaz8344 (2020).
34. Mimee, M. et al. An ingestible bacterial-electronic system to monitor gastrointestinal health. *Science* **360**, 915–918 (2018).
35. Bass, D. M., Prevo, M. & Waxman, D. S. Gastrointestinal safety of an extended-release, nondeformable, oral dosage form (OROS). *Drug Saf.* **25**, 1021–1033 (2002).
36. Isabella, V. M. et al. Development of a synthetic live bacterial therapeutic for the human metabolic disease phenylketonuria. *Nat. Biotechnol.* **36**, 857–864 (2018).
37. Bush, M., Ghosh, T., Tucker, N., Zhang, X. & Dixon, R. Transcriptional regulation by the dedicated nitric oxide sensor, NorR: a route towards NO detoxification. *Biochem. Soc. Trans.* **39**, 289–293 (2011).
38. Chen, X. J., Wang, B., Thompson, I. P. & Huang, W. E. Rational design and characterization of nitric oxide biosensors in *E. coli* Nissle 1917 and mini SimCells. *ACS Synth. Biol.* **10**, 2566–2578 (2021).

39. Ceze, L., Nivala, J. & Strauss, K. Molecular digital data storage using DNA. *Nat. Rev. Genet.* **20**, 456–466 (2019).
40. Beck, P. L. et al. Paradoxical roles of different nitric oxide synthase isoforms in colonic injury. *Am. J. Physiol.* **286**, 137–147 (2004).
41. Jiminez, J. A., Uwiera, T. C., Douglas Inglis, G. & Uwiera, R. R. E. Animal models to study acute and chronic intestinal inflammation in mammals. *Gut Pathog.* **7**, 29 (2015).
42. Strand-Amundsen, R. J. et al. Ischemia/reperfusion injury in porcine intestine—viability assessment. *World J. Gastroenterol.* **24**, 2009–2023 (2018).
43. Lundberg, J. O. N., Lundberg, J. M., Alving, K. & Hellström, P. M. Greatly increased luminal nitric oxide in ulcerative colitis. *Lancet* **344**, 1673–1674 (1994).
44. Liu, X. et al. Magnetic living hydrogels for intestinal localization, retention, and diagnosis. *Adv. Funct. Mater.* **31**, 2010918 (2021).
45. Song, M. et al. In *2020 IEEE International Solid- State Circuits Conference* 474–476 https://doi.org/10.1109/ISSCC19947.2020.9063083 (IEEE, 2020).
46. Krawczyk, K. et al. Electrogenetic cellular insulin release for real-time glycemic control in type 1 diabetic mice. *Science.* **368**, 993–1001 (2020).
47. Zhao, H. et al. Autonomous push button-controlled rapid insulin release from a piezoelectrically activated subcutaneous cell implant. *Sci. Adv.* **8**, 24 (2022).
48. Harimoto, T. et al. A programmable encapsulation system improves delivery of therapeutic bacteria in mice. *Nat. Biotechnol.* **40**, 1259–1269 (2022).
49. Li, Z. et al. Biofilm-inspired encapsulation of probiotics for the treatment of complex infections. *Adv. Mater.* **30**, e1803925 (2018).
50. Chen, W. et al. Bacteria-driven hypoxia targeting for combined biotherapy and photothermal therapy. *ACS Nano* **12**, 5995–6005 (2018).
51. Cao, Z., Wang, X., Pang, Y., Cheng, S. & Liu, J. Biointerfacial self-assembly generates lipid membrane coated bacteria for enhanced oral delivery and treatment. *Nat. Commun.* **10**, 5783 (2019).
52. Hu, Q. et al. Engineering nanoparticle-coated bacteria as oral DNA vaccines for cancer immunotherapy. *Nano Lett.* **15**, 2732–2739 (2015).
53. Vujkovic-cvijin, I. et al. Host variables confound gut microbiota studies of human disease. *Nature* **587**, 448–454 (2020).
54. Chiu, C. Y. & Miller, S. A. Clinical metagenomics. *Nat. Rev. Genet.* **20**, 341–355 (2019).
55. Steiger, C. et al. Ingestible electronics for diagnostics and therapy. *Nat. Rev. Mater.* **4**, 83–98 (2019).
56. Ma, Y., Selby, N. & Adib, F. Minding the billions: ultra-wideband localization for deployed RFID tags. In Proc. MobiCom '17 https://doi.org/10.1145/3117811.3117833 (Association for Computing Machinery, 2017).
57. Siuti, P., Yazbek, J. & Lu, T. K. Synthetic circuits integrating logic and memory in living cells. *Nat. Biotechnol.* **31**, 448–452 (2013).
58. Lloyd-Price, J., Abu-Ali, G. & Huttenhower, C. The healthy human microbiome. *Genome Med.* **8**, 51 (2016).
59. Inda, M. E., Mimee, M. & Lu, T. K. Cell-based biosensors for immunology, inflammation, and allergy. *J. Allerg. Clin. Immunol.* **144**, 645–647 (2019).

Methods

Bacterial strains and culture conditions

Routine cloning and plasmid propagation were performed in *E. coli* E. cloni 10G (Lucigen). For all in vitro and in vivo experiments, the probiotic strain *E. coli* Nissle 1917 was transformed with gene circuits built on plasmids and for the recombinase system, a bacterial artificial chromosome (BACs) was also used, as indicated in Supplementary Tables 2 and 3. Cells were routinely cultured at 37 °C in Luria–Bertani (LB) medium (Difco). Where appropriate, growth medium was supplemented with antibiotics at the following concentrations: 50 μg ml^{-1} kanamycin, 100 μg ml^{-1} carbenicillin, 25 μg ml^{-1} chloramphenicol, 100 μg ml^{-1} ampicillin and 100 μg ml^{-1} spectinomycin.

Plasmid construction and circuit characterization

All plasmids were constructed by combining PCR fragments generated by Phusion High-Fidelity DNA Polymerase (NEB) using Gibson assembly[60], starting from DNA sources as referenced in Supplementary Table 1, from gBlocks manufactured by IDT or acquired from Addgene. Genetic parts and plasmids used in this study are listed in Supplementary Tables 1 and 3, and are available from Addgene. Assembly products were introduced by transformation into chemically competent *E. coli* E. cloni 10G, and sequences were confirmed using Sanger sequencing.

To characterize the constructs built in conjunction with the memory system, appropriate antibiotics were added to Teknova Hi-Def Azure Media containing 0.2% glucose, and *E. coli* E. cloni 10G colonies were inoculated into this culture medium. Cultures were incubated aerobically with shaking for 16–18 h at 37 °C, then diluted 2,500× into fresh Hi-Def Azure Media (also containing appropriate antibiotics and 0.2% glucose) and incubated aerobically with shaking for another 20 min at 37 °C. Cultures (200 ml) were then transferred to a 96-well plate, and the respective inducers, H_2O_2 (hydrogen peroxide Sigma–Aldrich H1009-100ML), DETA–NO (Sigma–Aldrich D185-50MG), potassium tetrathionate (Sigma–Aldrich P2926-100G) and sodium thiosulfate (Sigma–Aldrich 217263-250G), were added at appropriate concentrations via serial dilution. Plates were incubated either aerobically with shaking or anaerobically for 20 h at 37 °C for all experiments. For experiments performed in anaerobic conditions, cultures were grown and manipulated in a Coy anaerobic chamber with an atmosphere of 85% N_2, 5% H_2 and 10% CO_2 at 37 °C. All media was pre-reduced overnight in anaerobic atmosphere before inoculation of cultures. After incubation, the optical densities of cultures were measured at 600 nm in a plate reader. For flow cytometry, cells were diluted in cold 1× PBS and 2% sucrose to reach an optical density of 0.02 (at 600 nm), then assayed on a BD LSRFortessa. A minimum of 10,000 gated events was recorded. BD FACSDiva 9.0 and FlowJo software v10 were used to export and process flow cytometry software files and analyse data and statistics. Forward scatter (FSC) and side scatter (SSC) were used to gate for cells excluding debris. The GFP emission was collected using the FITC detector with a 530/30 filter. Side scatter pulse height (SSC-H) was used to threshold on cells. Doublet gating was done on a SSC-W vs SSC-H plot, side scatter pulse width (SSC-W), as exemplified in Supplementary Fig. 1. Each experiment was performed with at least three biological replicates.

Growth and induction

For genetic circuit characterization, overnight cultures were diluted 1:100 in fresh LB and incubated with shaking at 37 °C for 2 h. Cultures were removed from the incubator and 200 μl of culture was transferred to a 96-well plate containing various concentrations of inducer. The plate was returned to a shaking incubator at 37 °C. Following 2 h of incubation, luminescence was read using a BioTek Synergy H1 Hybrid Reader with a 1 s integration time and a sensitivity of 150. Luminescence values, measured in relative luminescence units (RLU), were normalized by the optical density of the culture measured at 600 nm.

For in vitro kinetic studies, subcultured cells were mixed with an inducer in a 96-well plate and immediately placed in the plate reader set at 37 °C without shaking. Luminescence and absorbance were read at 3-min intervals.

Mouse experiments

Approval for mouse experiments was obtained from the Committee on Animal Care at the Massachusetts Institute of Technology. Male C57BL/6J mice (8–10 weeks of age) were obtained from Jackson Labs (stock no. 000664). Conventional conditions were used to house and handle the mice: 12/12 light cycle with 30–70% humidity and temp of 21 ± 1 °C; the mice were housed on ward wood shavings with reverse osmosis drinking water. One week before the experiments began, the mice were acclimatized to the animal facility.

Mice were randomly allocated to experimental groups. Researchers were not blinded to group assignments. Overnight cultures of *E. coli* Nissle 1917 grown in Teknova Hi-Def Azure Media with appropriate antibiotics and 0.2% glucose were centrifuged at 5,000*g* for 5 min and resuspended in an equal volume of 20% sucrose. Animals were inoculated with 200 μl of bacteria culture (approximately 10^8 colony-forming units (CFU)) by oral gavage. Faecal pellets were collected 6 h post-gavage[34], and homogenized in 1 ml PBS with a 5 mm stainless steel bead using a TissueLyser II (Qiagen) at 25 Hz for 2 min. Samples were centrifuged at 500*g* for 30 s to pellet large faecal debris. Supernatant was cultured in Teknova Hi-Def Azure Media with appropriate antibiotics and 0.2% glucose and incubated aerobically with shaking for 16–18 h at 37 °C. Cells were then assayed on the flow cytometer. For Extended Data Fig. 4d, carbenicillin and chloramphenicol were administered with the media for oral gavage. Where appropriate, growth media was supplemented with antibiotics at the following concentrations: 50 μg ml^{-1} kanamycin, 100 μg ml^{-1} carbenicillin, 25 μg ml^{-1} chloramphenicol, 100 μg ml^{-1} ampicillin and 100 μg ml^{-1} spectinomycin.

Pig experiments

Approval for pig experiments was obtained from the Committee on Animal Care at the Massachusetts Institute of Technology. Female Yorkshire pigs (50–95 kg), received from Cummings Veterinary School at Tufts University in Grafton, MA, were randomly selected for the experiments and housed under conventional conditions. Prior to the experiment, animals were given a clear liquid diet for 24 h. The day of the experiment, the morning feed was withheld. Pigs were sedated with Telazol (tiletamine plus zolazepam 5 mg kg^{-1}), xylazine (2 mg kg^{-1}) and atropine (0.04 mg kg^{-1}) at the start of the experiment. The jejunum was accessed via a midline laparotomy and the lumen sectioned into several test compartments using Mayo–Robson intestinal clamps. Ischaemia-reperfusion injury was used as a model of intestinal inflammation and was caused by clamping the mesentery of the target intestinal segment with haemostatic clamps for 2 h and then releasing the clamps to allow reperfusion for at least 1 h. At the end of the procedure, pigs were euthanized with Fatal Plus (sodium pentobarbital): 115–120 mg kg^{-1} and heart rate was assessed to ensure the pig was euthanized. For bacteria-only experiments, overnight bacterial cultures were diluted 1:10 in LB, cultured for 20 min, resuspended in 1 ml PBS after centrifugation and were injected into the target intestinal section via a syringe. Healthy intestinal sections were used as is or injected with 200 μl of the target analyte (DETA–NO, H_2O_2, tetrathionate or thiosulfate) as described in the text. After the experiment, cells were retrieved by flushing the intestinal section with 10 ml of PBS injected and retrieved via a syringe. For device bacteria experiments, overnight bacterial cultures were diluted 1:10 in LB, cultured for 20 min and 1 μl of fresh culture (concentrated 100× by centrifugation) was used to fill the pill casing chambers and sealed as described in 'Pill casing manufacture'. Devices were inserted into the intestinal lumen through a small incision, manually passed into the target intestinal section and isolated from

the incision site by luminal clamping as described above. Tetrathionate (100 mM) was injected via a syringe into the clamped intestinal compartment and data from the capsules was wirelessly acquired via a 915 MHz radio attached to a laptop (see Preparation of electronic components). Devices were manually retrieved from the jejunum. A total of three pigs were included in the experiments; three pigs on different days, two intestinal sections per animal, one for administering the inducer molecule and the other compartment as negative control.

Preparation of electronic components

The electronics in the capsules consisted of four photodiodes (Integrated CMOS P+/NWELL/PSUB photodiodes), a custom bioluminescence detector chip fabricated in a CMOS 65 nm process[2], a microcontroller (PIC12LF1840T39A, Microchip) and radio chip (PIC12LF1840T39A, Microchip Technology Inc.), and a 915 MHz chip antenna (0915AT43A0026, Johanson Technology). We used a commercial receiver (CC1200, Texas Instruments). The upper side of the top PCB holds the fully quartz lid-packaged CMOS chip together with an additional on-board LDO (ADP-166, Analog Devices). The assembly was coated with 1 µm of Parylene C to act as a moisture barrier for the electronic components. Parylene C coating was performed using Specialty Coating System Labcoter 2 (PDS 2010) with 1 g of dichlorodi-*p*-xylene to reach a target layer thickness of 1 µm as described[34].

Pill casing manufacture

Pill casing top and bottom blanks were printed by selective laser sintering in Grey resin on a Form 2 printer (Formlabs), post-processed according to the manufacturer's standard protocols and then flat outer faces were sanded to size. In the final design, Isopore membranes (0.4-µm pore size, Millipore-Sigma) were cut to size with a punch and then attached to the casing body via a thin, laser cut double-sided adhesive layer (3M VHB 5906). Unfilled pill casing tops were conditioned for 24 h in LB broth, and on the day of the experiment, the chambers were filled from the inside face with bacterial suspensions and subsequently sealed with a thin, laser cut, optically clear adhesive backing film (GeneMate Polyolefin Films with Silicone Adhesive). Bacteria-filled casing tops and empty bottoms were then pressed fit around the electronic system and the outer seam waterproofed with silicone (Elite Double 32, Zhermack). Porous membrane types were initially screened as described in Extended Data Fig. 6a using a standard two-chamber Franz cell. For experiments with enteric film-protected pill casings, the enteric films were solvent-cast from Eudragit L100-55 (Evonik Industries) plasticized with 50% w/w triethyl citrate and adhered to the outside of the capsule with a double-sided adhesive layer (3M VHB 5906) before loading the chambers with bacteria and without conditioning the capsules in LB.

In vitro device measurements

LB culture medium was pre-warmed for at least 2 h prior to the start of experiments. For device-bacterial experiments, overnight cultures were diluted 1:10 in LB, subcultured for 20 min, and concentrated 100× by centrifugation. One microlitre of the concentrated culture (~10^{10}–10^{11} CFU ml^{-1}) was then added to pill casing chambers. Wild-type *E. coli* Nissle 1917 was added to the reference channel for all experiments. Once all four channels were loaded, the cell carrier was fastened to the capsule and fully submerged in pre-warmed media. LB culture media supplemented with inducer (100 mM tetrathionate). Cultures were wrapped several times in thick black fabric to block external light and placed in an incubator at 37 °C, and data was collected wirelessly for 2 h. At the end of the experiment, devices were disassembled and cell carriers were discarded. Capsules were sterilized with 70% ethanol and thoroughly washed with distilled water. Capsules were left to air-dry and re-used for future experiments.

In vitro device viability and luminescence measurements after simulated ingestion

Devices were loaded with 2 µl of bacteria as described above using a strain of *E. coli* Nissle 1917 carrying a plasmid with constitutive expression of the luciferase reporter operon (sMJD026). Enteric-film protected devices and unprotected devices were submerged in simulated gastric fluid (USP, pH 1.2, no enzymes) and/or simulated intestinal fluid (USP, pH 6.8, no enzymes) and incubated at 37 °C in a tube revolver on oscillating mode (Thermo Scientific, 88881001) for the indicated time (Extended Data Fig. 7) to simulate ingestion and transit through the stomach. Following incubations, chambers were dried, and the luminescence signal was recorded (ChemiDoc, BioRad) and quantified using FIJI (ImageJ) as described in (Extended Data Fig. 7). Then the optically clear adhesive backing film was removed, 1-µl samples of each chamber were retrieved, serially diluted in PBS and spotted onto LB agar plates with a pin replicator (V&P Scientific, VP 407A). Given a transfer volume of ~1.5 µl, dilutions with countable colonies (between 1–20) were used to determine the CFU per ml in the initial chamber volume.

Radio frequency experiments

In order to test wireless transmission in water, the device was immersed in water in a 1 l beaker (deposited in the middle, diameter 10 cm) and we could measure a wireless power of −70 dBm, which is well above the sensitivity limit of −110 dBm as informed in the datasheet of the receiver (CC1120, Texas Instruments). This confirms that the wireless signal can be transmitted at least 5 cm (half diameter) through water, with significant (40 dB) link margin left over.

Additionally, when the same wireless transmitter (PIC12LF1840T39A, Microchip) was placed fully inside the cavity of an anaesthetized pig, a signal could be detected with the receiver (CC1120, Texas Instruments) 5 m from the animal. When the integrated testing device was placed in the intestine inside of an anaesthetized pig, we could regularly measure a wireless power ranging between −90 dBm to −100 dBm (which is above the sensitivity limit) when the receiver was 1 m from the animal.

Calibration procedure for converting detector counts to estimated photocurrent

One-time optical calibration was performed to obtain the custom integrated circuit (IC) performance and calibration parameters. During the optical calibration, the wireless capsule holding the custom luminescence detector IC, a standalone photodiode IC, and a green LED (λ = 520 nm) were placed inside a metal box covered by a blackout cloth to prevent ambient light from the environment. The capsule and the standalone photodiode IC were placed 1.5 cm adjacent to each other on one side of the metal box, while the LED was placed 30 cm opposite both ICs on the other side of the metal box. We applied 5 different voltage levels (0 V, 2.1 V, 2.14 V, 2.165 V, 2.185 V) across the LED to obtain different optical power levels. The custom luminescence detector IC[2] wirelessly transmitted sensor readout N_i for each sensing channel i at a given optical power. The standalone photodiode IC was exposed to this optical power simultaneously, and the IC reported a photocurrent level I_{PD} through a sub-femtoamp SourceMeter (K6430, Keithley Instruments). The resolution of a sensing channel i is defined as:

$$\text{Resolution} = \Delta I_{PD}/\Delta N_i$$

where ΔI_{PD} is the difference between photocurrent values reported from the standalone photodiode IC for two LED bias voltages; and ΔN_i is the difference between luminescence detector IC output counts for the same LED bias voltages. The resolution for a single channel was calculated using a linear regression model to fit the luminescence IC output counts and photocurrents from standalone photodiode IC over five LED bias voltages. The resolution of the luminescence detector chip is 5.8–6.5 fA per count. The minimum detectable signal at one

LED bias voltage was calculated using the resolution of each sensing channel times one standard deviation of the IC output at this optical power. The worst-case minimum detectable signal is 71 fA. The estimated photocurrents for in vitro and in vivo measurements were calculated by taking the product of resolutions from one-time optical calibration and measured IC output counts in each measurement. We used a moving average filter of 25 samples (~15 min moving average).

Data analysis, statistics and computational methods

All data were analysed using GraphPad Prism version 9.1.2 (GraphPad Software). Sequences were analysed using SnapGene version 5.1.2 (www.snapgene.com). As noted, error bars represent the s.e.m. of at least three independent experiments carried out on different days. Significant differences between groups was determined using an unpaired, two-tailed Student's *t*-test assuming unequal variance and for curves over time, two-way ANOVA for multiple comparisons. Fold change or SNR was determined by dividing the normalized luminescence values (divided by optical density) of samples treated with the maximal inducer concentration with uninduced samples. The ROC was calculated based on multiple independent experiments ($n = 5$ for tetrathionate and $n = 3$ for buffer compartments). Parts of the figures were drawn using images ('complete digestive apparatus', 'multi-well plate', 'pig', 'rodents', 'Bacteriology_virology' and 'Blood_immunology') from Servier Medical Art. Servier Medical Art by Servier is licensed under a Creative Commons Attribution 3.0 Unported License (https://creativecommons.org/licenses/by/3.0/). We used Cadence IC 6.1.7 for circuit design, layout design and simulations (https://www.cadence.com/en_US/home.html), and Calibre 2016 for circuit verification (https://eda.sw.siemens.com/en-US/ic/calibre-design/circuit-verification/).

Reporting summary

Further information on research design is available in the Nature Portfolio Reporting Summary linked to this article.

Data availability

All data are provided in the paper and in the supplementary information. Genetic sequences and plasmids have been deposited into the Addgene repository under Addgene identifiers 199782–199792.

60. Gibson, D. G. et al. Enzymatic assembly of DNA molecules up to several hundred kilobases. *Nat. Methods* **6**, 343–345 (2009).
61. Reinders, C. I. et al. Rectal mucosal nitric oxide in differentiation of inflammatory bowel disease and irritable bowel syndrome. *Clin. Gastroenterol. Hepatol.* **3**, 777–783 (2005).

Acknowledgements This work was supported by Leona M. and Harry B. Helmsley Charitable Trust (3239), Pew Charitable Trusts (to M.E.I.-W.; 00030623) and Catalyst Foundation (to R.T.Y., Q.L. and M.E.I.-W.; Secure Bio-Engineered Sensors for Disease Management, SAP grant no. 55208844). M.J. was supported by the Translational Research Institute of Space Health through Cooperative Agreement NNX16AO69A. G.T. was supported in part by the Department of Mechanical Engineering, MIT and the Karl van Tassel (1925) Career Development Professorship, MIT. Part of this material is based on research sponsored by 711 Human Performance Wing (HPW) and Defense Advanced Research Projects Agency (DARPA) under agreement number FA8650-21-2-7120. The US Government is authorized to reproduce and distribute reprints for governmental purposes notwithstanding any copyright notation thereon. The views and conclusions contained herein are those of the authors and should not be interpreted as necessarily representing the official policies or endorsements, either expressed or implied, of 711 Human Performance Wing (HPW) and Defense Advanced Research Projects Agency (DARPA) or the US Government.

Author contributions M.E.I.-W., M.J., Q.L., N.V.P., C.S., M.M., P.N., G.T., R.T.Y. and T.K.L. conceived and designed the research. M.E.I.-W., M.J., Q.L., C.S., A.W., M.M., P.N., A.P.C., G.T., R.T.Y. and T.K.L. conceptualized the miniaturized pill form factor, including integration of the bacteria, electronics and pill casings. M.E.I.-W. designed and performed in vitro biological experiments. Q.L., A.R. and T.Z. designed and built the integrated electronic circuits. M.E.I.-W. designed and performed in vivo mouse experiments. M.J., J.A., A.W. and K.W. developed the pill casing manufacturing process and validated the pill casing robustness in vitro, including membrane attachment. M.J., A.W., K.W. and R.M. generated 3D-printed device components. M.J. developed and validated the free-standing enteric films. M.E.I.-W., M.J., Q.L., N.V.P., C.S., A.H. and GT validated early prototypes. M.J., N.V.P., C.S., K.I., J.J., J.K., A.H. and G.T. conceptualized and validated the intestinal compartment animal model. K.I., N.F., J.J., J.K., A.H. and W.M. carried out animal husbandry and anaesthesia of pigs. M.E.I.-W., M.J. and Q.L. experimentally tested the function of the integrated devices in vitro and in vivo. M.E.I.-W., M.J. and Q.L. performed formal analysis of the data. M.E.I.-W., M.J., Q.L., J.A., P.N. and R.T.Y. contributed to data analysis of in vitro and in vivo experiments of the integrated devices. M.E.I.-W., M.J., Q.L., N.V.P., J.A., A.W., P.N. and R.T.Y. contributed to visualization. M.E.I.-W., M.J., Q.L., M.M., P.N., A.P.C., G.T., R.T.Y. and T.K.L. wrote the manuscript. M.E.I.-W., M.J., Q.L., P.N., C.S., A.W., A.H., G.T. and R.T.Y. managed daily project progress and personnel. M.E.I.-W. and T.K.L. supervised and managed general project administration. R.T.Y., G.T. supervised and managed funding of the project related to the integrated electronics and integrated pill casings and swine husbandry, respectively. M.E.I.-W., M.J., N.V.P., C.S., Y.L., M.M., P.N., A.P.C., R.T.Y., G.T. and T.K.L. contributed with funding acquisition.

Competing interests MIT and Boston University have filed a Patent Cooperation Treaty (PCT) patent application (WO/2022/232188) regarding ingestible biosensors and methods of their use. T.K.L. is a co-founder of Senti Biosciences, Synlogic, Engine Biosciences, Tango Therapeutics, Corvium, BiomX, Eligo Biosciences and Bota.Bio. T.K.L. also holds financial interests in nest.bio, Ampliphi, IndieBio, MedicusTek, Quark Biosciences, Personal Genomics, Thryve, Lexent Bio, MitoLab, Vulcan and Serotiny. A.P.C. is on the board of Analog Devices. M.J. consults for VitaKey. C.S. is currently employed by Bayer AG (Germany). Complete details of all relationships for profit and not for profit for G.T. can found at https://www.dropbox.com/sh/szi7vnr4a2ajb56/AABs5N5i0q9AfT1IqIJAE-T5a?dl=0.

Additional information

Supplementary information The online version contains supplementary material available at https://doi.org/10.1038/s41586-023-06369-x.

Correspondence and requests for materials should be addressed to G. Traverso, R. T. Yazicigil or T. K. Lu.

Peer review information *Nature* thanks Jeff Hasty and the other, anonymous, reviewer(s) for their contribution to the peer review of this work. Peer review reports are available.

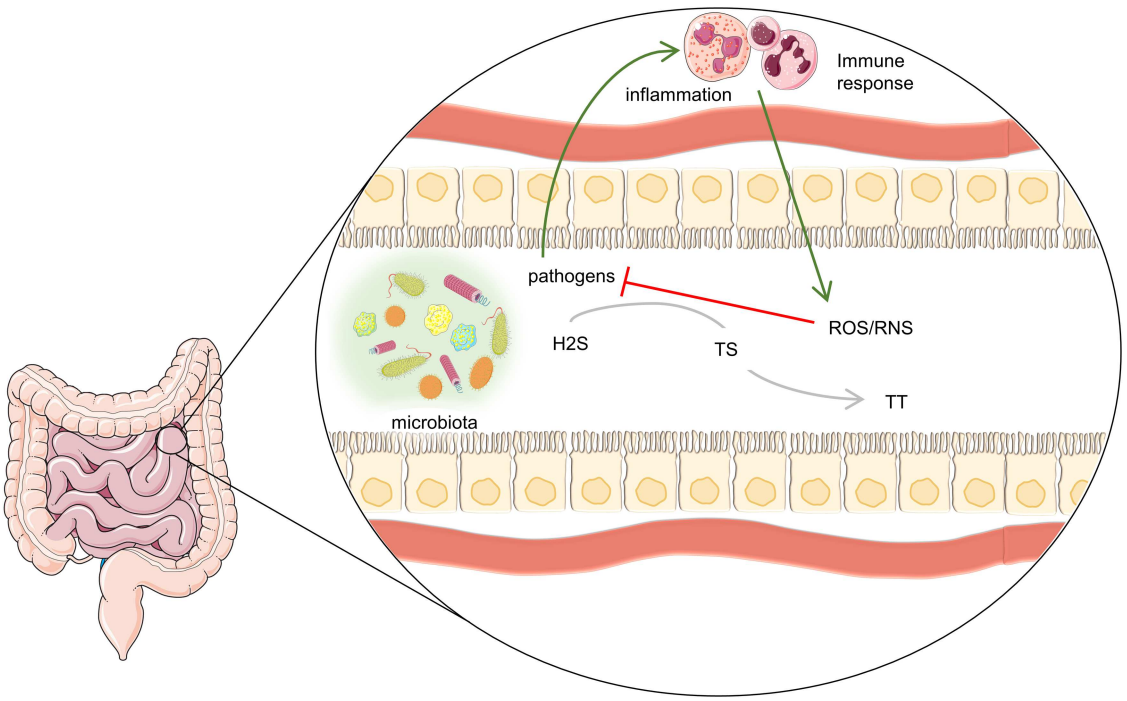

Extended Data Fig. 1 | Inflammatory bowel disease (IBD) is mediated by labile molecules that are not detectable with current technologies. Following an inflammatory insult, disproportionate mucosal immune responses via cytokine signaling lead to the release of redox-active molecules such as reactive oxygen species (ROS) and nitric oxide (NO). The resulting oxidative stress inhibits microbial growth in the gut lumen. However, chronic intestinal inflammation damages the epithelium and destroys the epithelial barrier, allowing intestinal microbes to invade the mucosa. The sources of thiosulfate (TS) in the GI tract are mucin-derived cysteine and sulfate, which are metabolized to hydrogen sulfide (H_2S)[19]. During ulceration, epithelial cells and red blood cells enter the colon; these cells produce enzymes that convert H_2S to TS. In the presence of ROS, TS is oxidized to tetrathionate (TT). Consumption of TT and sulfate allows certain pathogens to establish a foot-hold for infection[19,29], evoking further immune responses. These mediators of disease are labile and cannot be measured with existing technology. With only the limited information current approaches provide, breaking this positive feedback loop is challenging.

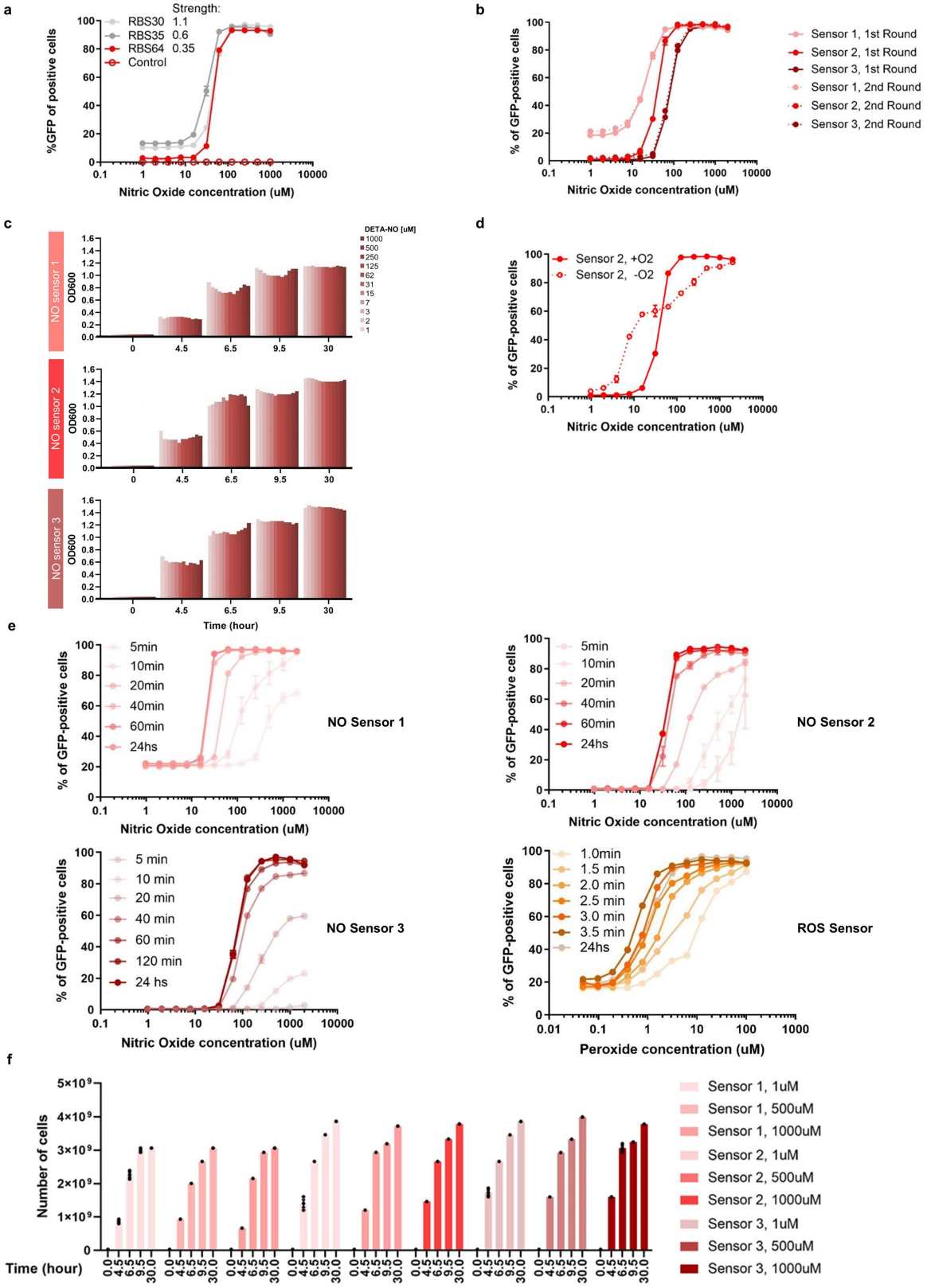

Extended Data Fig. 2 | See next page for caption.

Extended Data Fig. 2 | Genetic circuit optimization and characterization of incorporated recombinase-based switch. a, Dose-response curves of NO-sensing genetic circuits in *E. coli* Nissle 1917. The translational initiation strength of the recombinase Bxb1 was varied by using different computationally designed ribosome binding sites (RBS). Predicted RBS strengths are listed in the inset. Lower RBS strength led to a higher SNR. **b**, The memory circuit in the three NO sensors was stable over multiple rounds of re-growth. Engineered bacteria collected in stool were cultured in a selective media to measure NO detection, and the memory system was validated to ascertain that it accurately reflected, over multiple rounds of culturing, the initial input. **c**, GFP expression did not affect growth of bacteria when ON vs. OFF states were compared. **d**, NO detection in anaerobiosis. **e**, Time course of switch activation. The recombinase system triggered GFP expression within minutes (5 min for sensor NO Sensor 1 and NO Sensor 2, 10 min for NO Sensor 3, and less than 1 min for the ROS sensor) of exposure to the target molecule. **f**, Correlation of number of cells, time and concentration to show the performance of the system, (n = 3 per group). Lines represent the mean. Data are represented as mean ± SEM of three independent biological replicates derived from flow cytometry experiments (a–b, d–e), each of which involved n = 10,000 events.

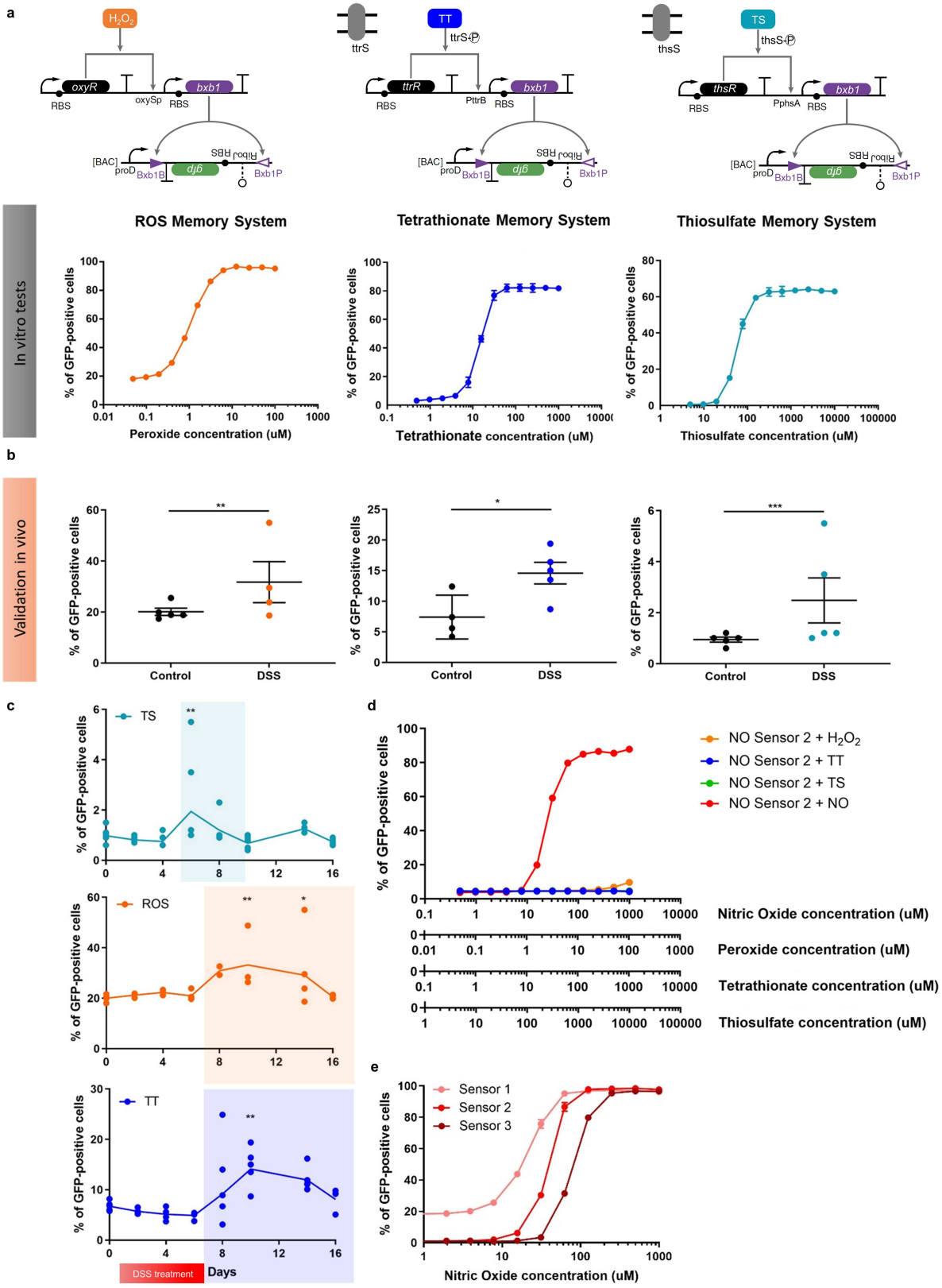

Extended Data Fig. 3 | See next page for caption.

Extended Data Fig. 3 | Multiple specific disease biomarkers detected in vitro and in vivo. a–c, The bacterial sensors were validated for the ROS H_2O_2, TS, and TT in vitro (a,d) and in vivo (b–c), following the protocol shown in Fig. 2. In the presence of H_2O_2, the transcription factor OxyR is oxidized and activated in *E. coli*. To construct a ROS biosensor that detected H_2O_2, the recombinase gene *bxb1* was placed under the control of the OxyR-regulated oxyS promoter, oxySp, on the same genetic circuit[18] (panel a). To construct the TT and TS sensors, we sought to overcome the oxygen repression that can affect Fumarate and Nitrate Reductase Regulator (FNR)-dependent sensors such as the previously reported two-component system TtrSR[29]. Oxygen levels fluctuate in the gut, depending on the level of disruption of the mucosal epithelium. To avoid this cross-repression, we used two newly identified sensors to express the recombinase system for detecting TS and TT: a TT sensor from *Shewanella baltica*, which does not depend on the FNR system, and the ThsRS sensor from *Shewanella halifaxensis*, the only genetically encoded TS sensor characterized so far[19]. Both sensors distinguished their target molecules from other terminal electron acceptors in vitro[19]. **d**, The cross-reactivity of the NorR-engineered bacteria was tested against ROS (H_2O_2), TT and TS in a series of dose-response curves (series of two-fold dilutions of the inducer with an initial concentration of 0.1 mM, 1 mM and 10mM respectively and 1mM for the positive control with DETA-NO). In (a and d) lines represent the mean, the errors (SEM) are derived from flow cytometry experiments of three representative biological replicates, each of which involved n = 10,000 events. In (b-c) individual points represent independent biological replicates, n = 5 animals per group, and the bars (b), **p = 0.0091 (ROS, day 14), *p = 0.0243 (TT, day 10), ***p = 0.0006 (TS, day 6), and lines (c) show the mean with SEM, **p = 0.0011 (TS, day 6), **p = 0.0029 (ROS, day 10), *p = 0.0126 (ROS, day 14), **p = 0.0053 (TT, day 10), two-way ANOVA for multiple comparisons. **e**, The NO biosensor was evaluated for its use as an NO disease stage detector. NorR, constitutively expressed from a library of ribosome-binding sites (RBS), exhibited different NO activation thresholds. Selected NO sensors (Sensor 1, 2, and 3) detected three concentrations (15, 30, and 80uM), which could correspond respectively to mild, moderate, and severe states of inflammation[61]. Based on the recombinase system described in Fig. 2a, flow cytometry was used to measure the percentage of GFP-positive cells at different concentrations of NO. For each point, the mean of three biological replicates, each with n = 10,000 flow cytometry events, is plotted. Error bars are the standard error of the mean (SEM).

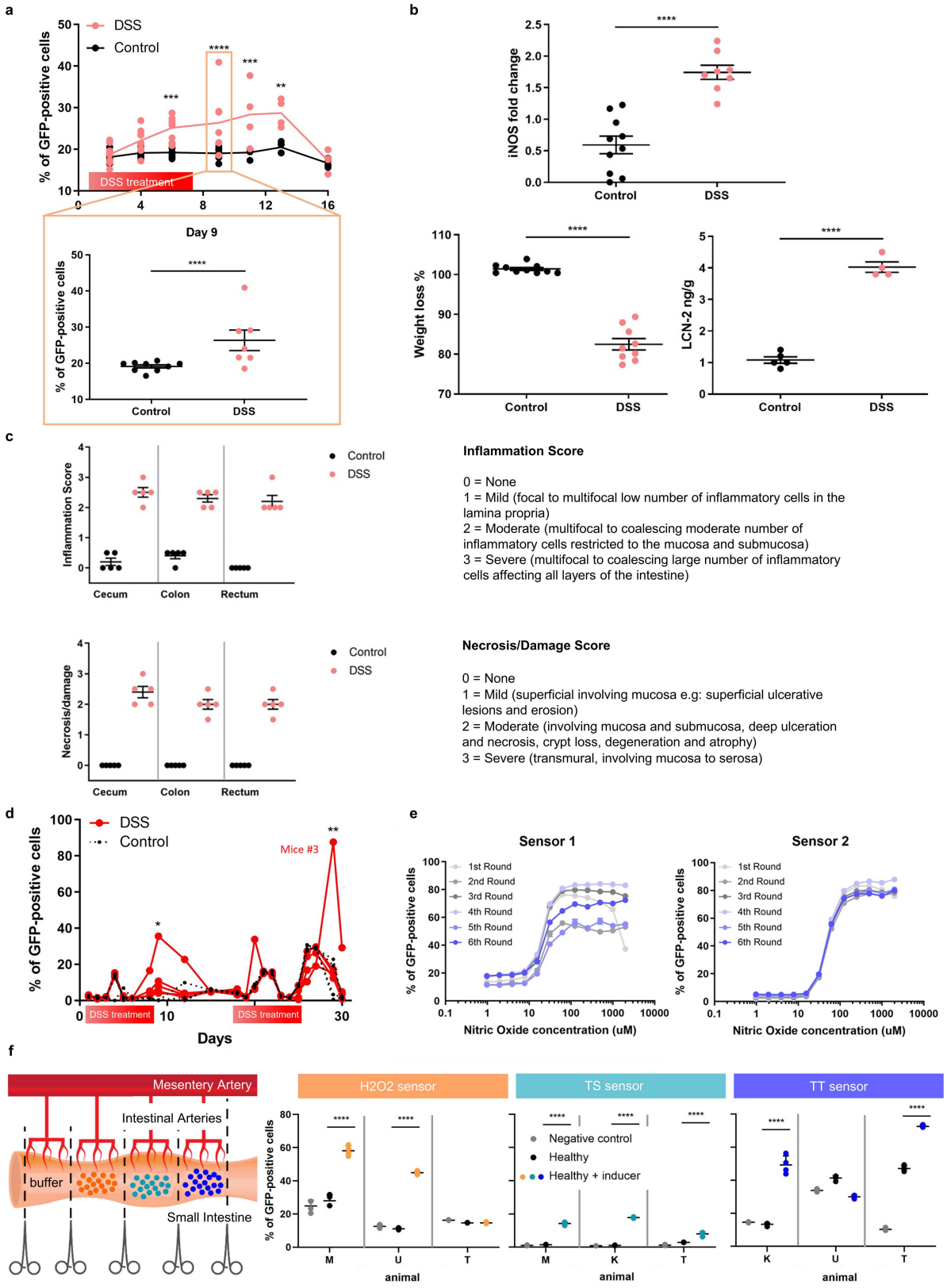

Extended Data Fig. 4 | See next page for caption.

Extended Data Fig. 4 | In vivo validation of inflammatory biosensors. **a**, Detection of NO by the NO biosensor as a marker of GI inflammation in vivo over time, n = 10 animals per group. Data are represented as mean ± SEM, **p = 0.0012 (day 13), ***p = 0.0005 (day 6), ***p = 0.0002 (day 11), ****p < 0.0001 (day 9), two-way ANOVA for multiple comparisons. **b**, Independent validation of the presence of inflammation in the DSS colitis model by quantifying iNOS expression during DSS treatment, weight loss, and the lipocalin-2 (LCN-2) biomarker, n = 10 animals per group. Data are represented as mean ± SEM, ****p < 0.0001, two-tailed unpaired Student's t test. **c**, Histological scores of inflammation and necrosis, indicating the validity of the DSS model. Other indicators were observed but not quantified: bloody and loose stools, poor vigor, anal prolapse, and shortening of the colon upon dissection and gross morphological examination. Lines represent the mean. Error bars represent the SEM of independent biological replicates. **d**, Antibiotic-triggered redox imbalance measured by the NO sensor. NO Sensor 2 allowed us to detect an exacerbated inflammatory response after antibiotic treatment (carbenicillin and chloramphenicol) in a chronic DSS inflammation model, which implies multiple rounds of DSS treatment. Our biosensor for NO shows an increase of NO expression after 4 and 20–30 days of antibiotic treatment in both healthy and DSS-treated mice, with a significant switch activation on day 9 in the DSS-treated mice and on day 29 in the chronic DSS inflammation model, especially high for mouse #3. 'DSS" samples, n = 5 and "Control" samples, n = 5. *p = 0.0408, **p = 0.0038, two-way ANOVA for multiple comparisons. **e**, Control for basal % of GFP+ over 4 days. After six rounds of re-growth of Sensor 1 and Sensor 2, the background signal of non-induced cells does not continue expanding over time, which validates them for use in animal models. Engineered bacteria were cultured in a selective media to measure NO detection, and the memory system was validated to ascertain that it accurately reflected, over multiple rounds of culturing (6 rounds, during 4 days) the initial input, n = 3 per group. Data are represented as mean ± SEM. **f**, Sensor validation in pigs. Experimental design: intestines were clamped to separate the different compartments (control vs. treated), and bacterial sensors were placed in the different compartments (left panel). All sensors registered significant activation in the presence of their respective inducers (300 uM H_2O_2, 30 mM TS, 3 mM TT, right panel). The bacteria were collected from the intestine after two hours of exposure to the analyte, and the percentage of GFP-positive cells was measured by flow cytometry. Lines represent the mean. The errors (SEM) are derived from flow cytometry experiments of three representative biological replicates, each of which involved n = 10,000 events. Here, we show data of three independent experiments (three animals [M, U, T, K] on different days, multiple compartments per animal). ****p < 0.0001, two-way ANOVA for multiple comparisons.

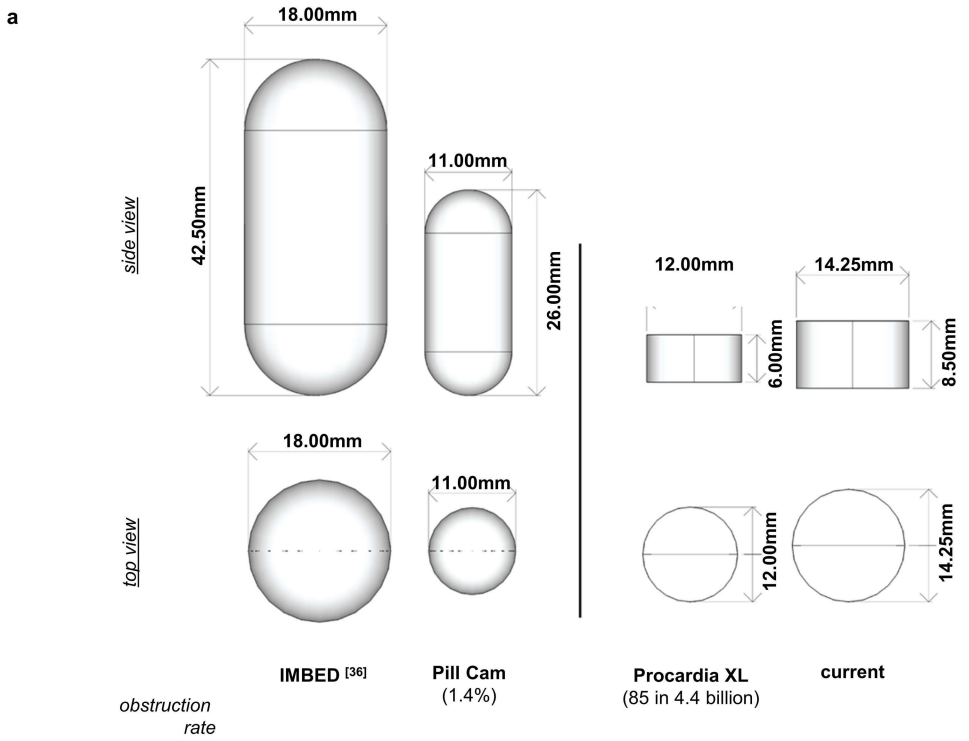

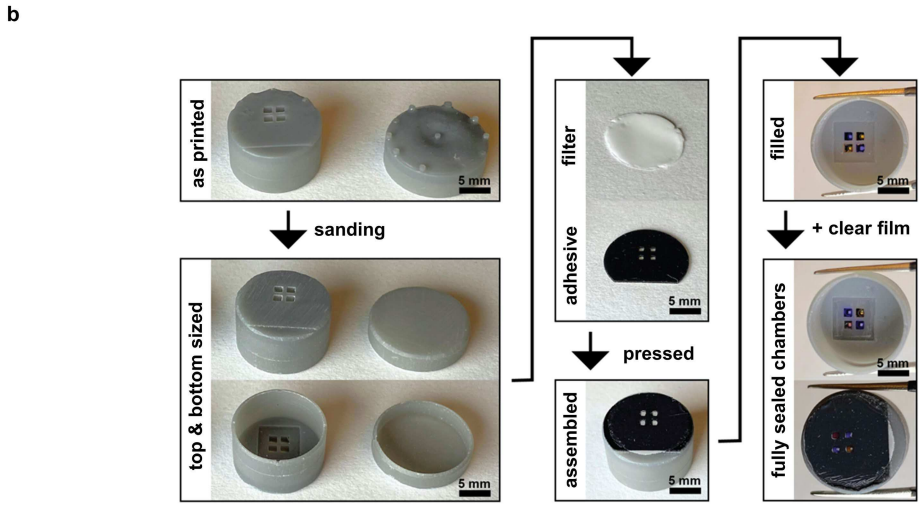

Extended Data Fig. 5 | Design and manufacture of a bacteria-electronic pill casing compatible with ingestion. a, Size comparison of ingestible electronics and solid dosage forms with established safety rates. The safety of ingestible devices depends, in part, on ensuring that these devices will not damage, obstruct, or be retained in the GI tract. The current design was built to conform with the dimensions and form factors of solid dosage forms with known safety profiles and obstruction/retention rates (Procardia XL)[55]. Our system integration at the bacterial, electronics, and pill casing level allowed a significant reduction in size compared to a previously reported prototype (>9 mL to <1.4 mL)[34]. **b**, **Pill casing manufacturing process.** Casing blanks are 3D printed via selective laser sintering (Formlabs) with supports only on the top and bottom face to preserve the thin wall features. The top and bottom faces are then sanded to size. The filter membrane is cut to size with a punch and the double-sided adhesive film is laser cut with through holes aligned to the chambers. After pressing these outer layers together, the chambers are filled with bacterial suspensions from the inside and sealed off with a thin clear adhesive film to yield the fully sealed bacterial chamber/casing unibody. Scale bar = 5 mm.

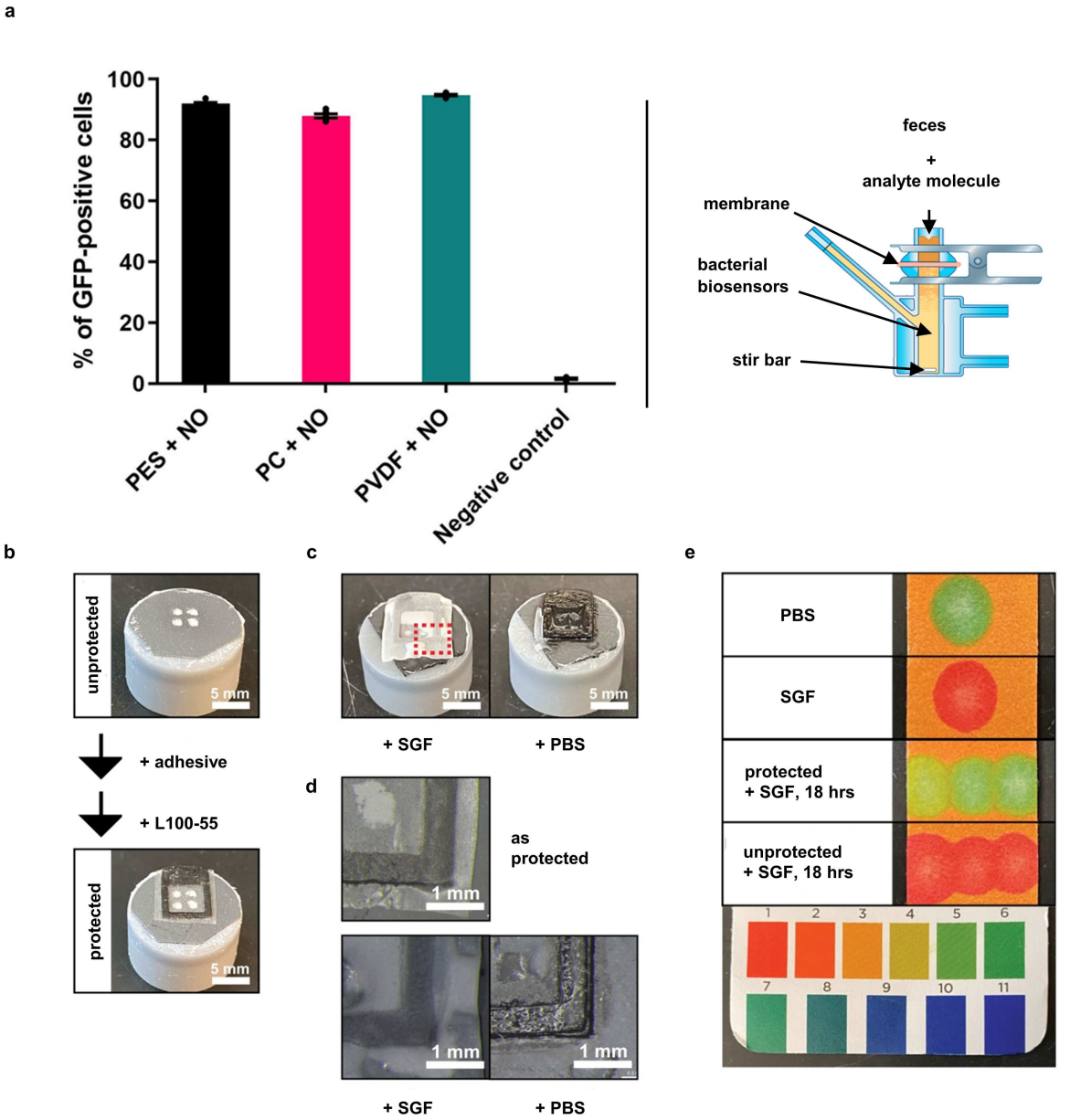

Extended Data Fig. 6 | Validation of semipermeable membranes and coatings for sealing and protection of on-board bacterial sensors. a, Effect of membrane on analyte diffusion. The porous membranes, when placed in feces, did not interfere with detection of the target molecules. Fouling of the membrane by faecal matter may pose a problem, so we also screened several membrane materials, e.g., polyethersulfone (PES), polycarbonate (PC), and polyvinylidene fluoride (PVDF), to find which material allowed the highest diffusion of the analyte molecules across the membrane. Several porous membranes were tested in Franz Cells (inset on the right) in the presence of feces. All the membranes tested showed similar results, with a similar percentage of detection from the NO bacterial sensors after the analyte had passed through the membrane. The errors (SEM) are derived from flow cytometry experiments of three representative biological replicates, each of which involved n = 10,000 events. **b**–**e**, **Manufacturing and performance of a pill casing protected from low pH ingress, compatible with ingestion**. **b**, The assembled pill casing/chamber unibody can protect the sensor bacteria against low pH during stomach transit by inclusion of a film made of an enteric polymer (L100-55) attached via an adhesive layer (black). **c**, The enteric film hardens after exposure to simulated gastric fluid (SGF), but dissolves away after a brief exposure (< 1 hr) to neutral pH (PBS) allowing the bacteria to be exposed to the chemical environment of the small intestine. **d**, close-up view (red, dashed square in panel b) of enteric protected pill casings showing no membrane fouling after exposure to neutral pH (PBS). **e**, analysis of internal pH of fluid inside casing chambers by spotting contents onto pH paper. First two rows are control spots of the indicated fluids. Last two rows are spots from three chambers each from a protected or un-protected pill casing exposed to simulated gastric fluid (SGF) for 18 h. Bottom legend indicates corresponding pH of the resulting color change.

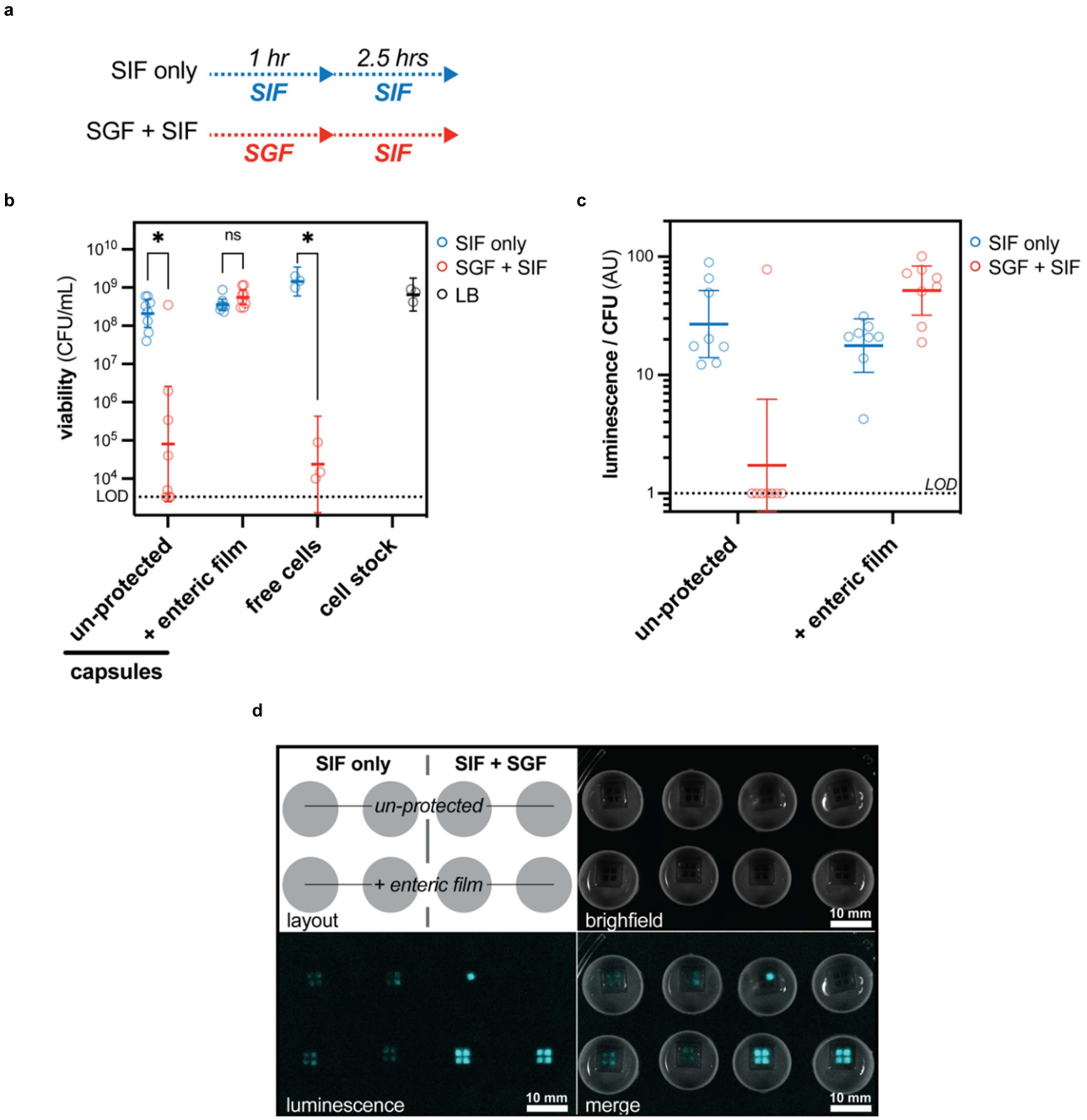

Extended Data Fig. 7 | Enteric-protected pill casings preserve viability and luminescence of on-board bacterial sensors through simulated ingestion. **a**, Un-protected or enteric-protected pill casings were loaded with constitutively luminescent bacterial cells and exposed to simulated intestinal fluid (SIF only, blue) or simulated ingestion with a 1-hour exposure to pH 1.2 simulated gastric fluid (SGF+SIF) at 37 C. **b**, At end of exposure the internal chamber contents were extracted and viability was measured through serial dilution and colony counting. As a control, an equivalent number of cells was directly resuspended in the exposure fluids (free cells) and pelleted between treatments. The viability of the common cell stock used to load the pill casings and for the free cell control was kept refrigerated during the exposures and its viability was also measured. Geometric mean and geometric 95% confidence intervals are plotted on top of individual replicate chambers. N = 8 (4 chambers x 2 pill casings), Multiple unpaired t-tests (two-tailed), *p = 0.0253 (unprotected), *p = 0.0195 (free cells), (ns) not significant. **c**, At end of exposure, the luminescence of the same chambers was also recorded (BioRad, ChemiDoc) from the inner side of the casings through the optically clear backing film. Total chamber luminescence was quantified (FIJI, ImageJ) and divided by the total chamber colony forming units (CFU) from panel b. The limit of detection (LOD) was set at 2.5x the standard deviation of the background signal divided by the largest viability value observed. Values below the LOD were set equal to the LOD and all values were normalized to set the LOD = 1. Geometric mean and geometric 95% confidence intervals are plotted on top of individual replicate chambers. N = 8 (4 chambers x 2 pill casings). **d**, Images used for luminescence quantification in panel c.

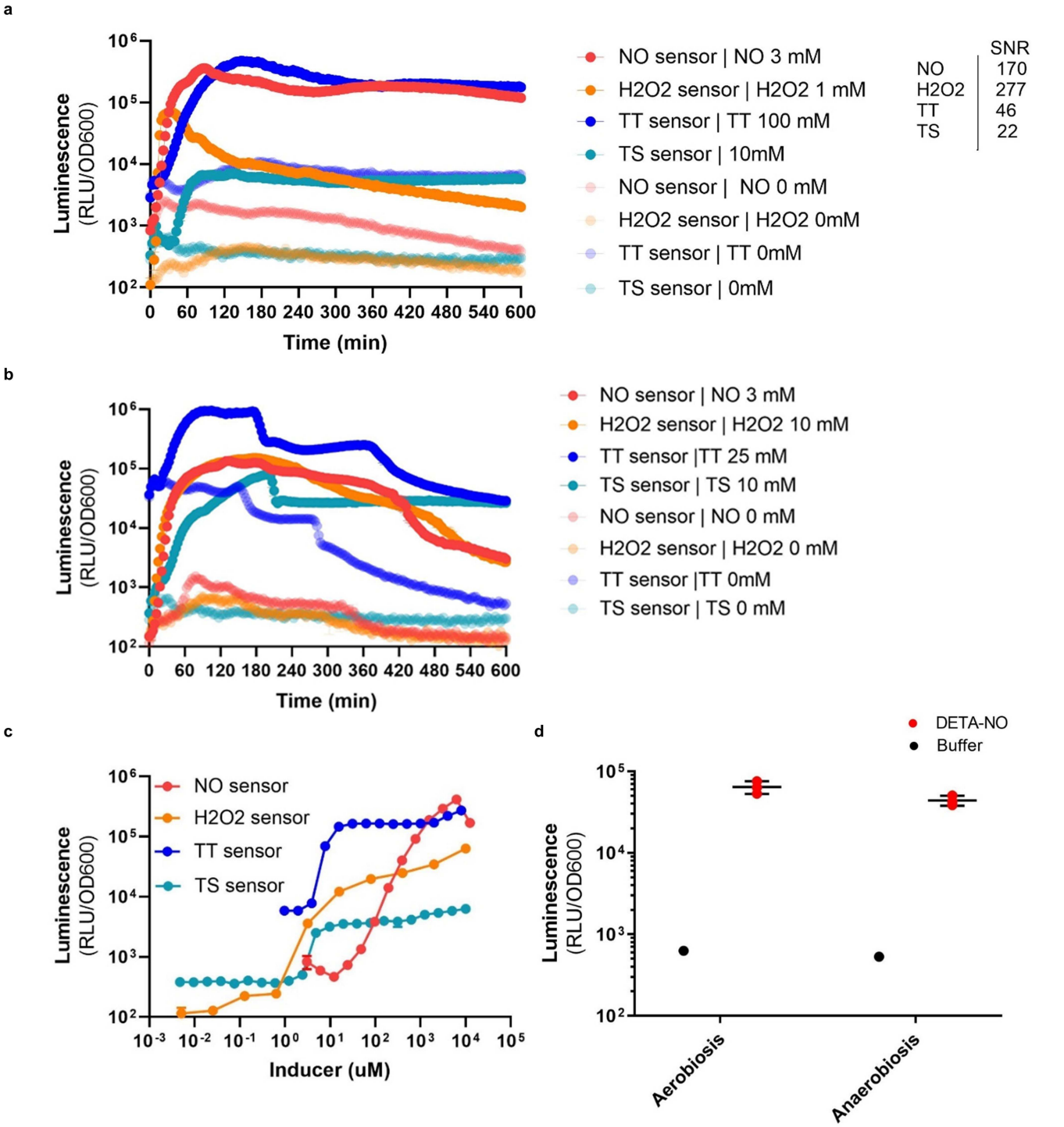

Extended Data Fig. 8 | Kinetic response of the inflammatory biosensors with the luciferase readout. a–**b**, *E. coli* Nissle biosensors were treated with their target analytes in LB (a) or in simulated intestinal fluid (b). The luminescence response was measured in a plate reader every 3 min for 10 h. The signal-to-noise ratio (SNR) was calculated by dividing the OD600-normalized luminescence values induced by the OD600-normalized luminescence values of uninduced samples. **c**, Response curve of the inflammatory biosensors with the luciferase readout. *E. coli* Nissle inflammatory sensor strains were treated with various concentrations of their target analytes; maximal luminescence values were measured thirty minutes to two hours post-exposure to the inducer and normalized to the optical density of the culture. Lines represent the mean. Error bars represent the SEM of three independent biological experiments. **d**, Nitric oxide (NO) detection and luciferase expression in anaerobiosis, replicating the gut environment. Luminescence values were measured aerobically in a plate reader after overnight aerobic or anaerobic growth and exposure to the inducer (DETA-NO 1mM) and normalized to the optical density of the culture. Lines represent the mean. Error bars denote the SEM for three independent biological replicates.

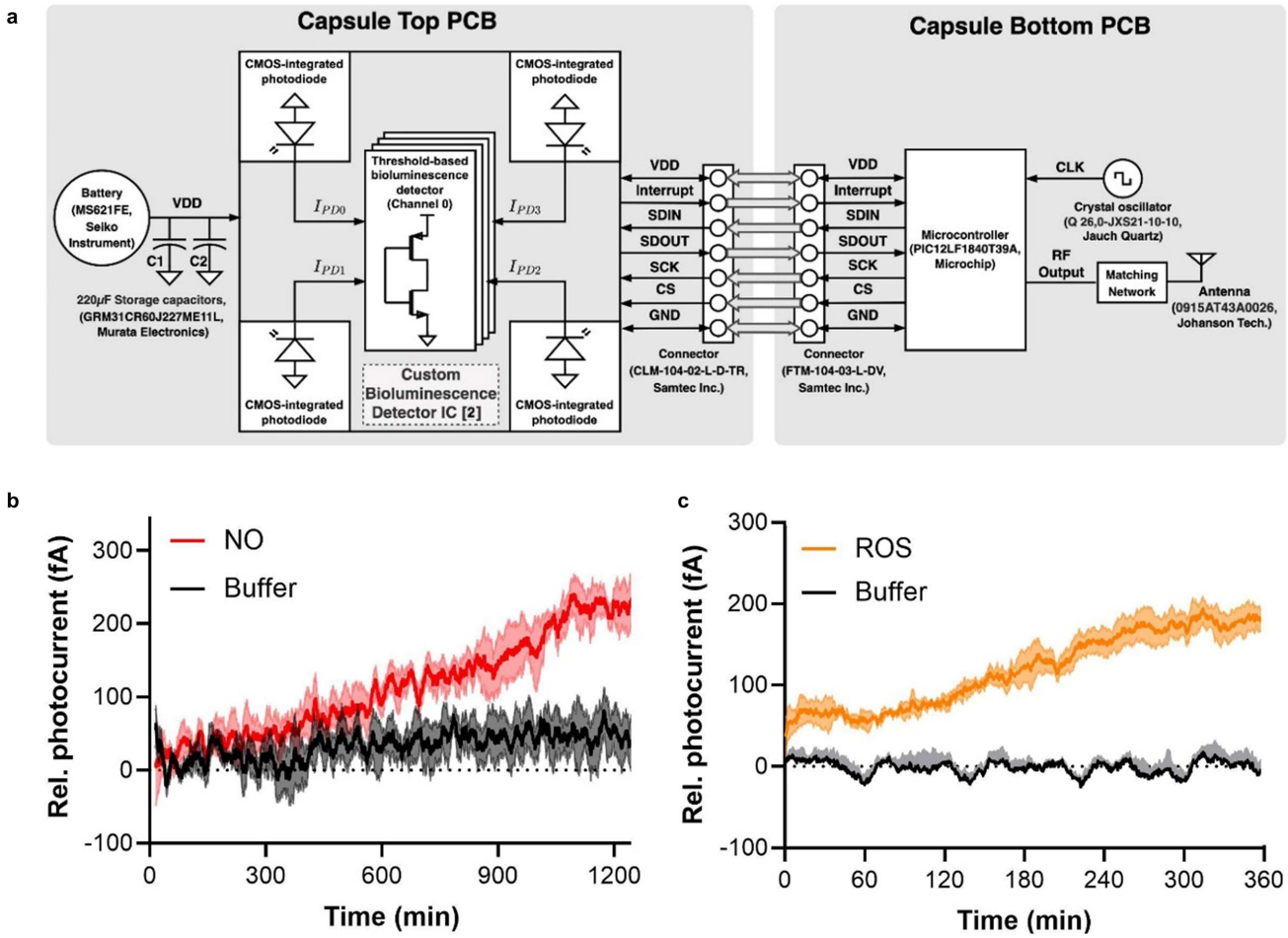

Extended Data Fig. 9 | Electronic design and in vitro validation of the integrated bacterial-electronic pill. a, Schematic of the miniaturized capsule PCB. The custom bioluminescence detector IC was fabricated in 65 nm CMOS technology[2]. The top PCB holds the custom-designed multi-channel and time-multiplexed bioluminescence detector, a 6.8 mm x 2.1 mm coin-cell battery, two 220 μF decoupling capacitors, and an 8-position female connector. The bottom PCB holds a microcontroller with an integrated transmitter, a crystal oscillator, an 8-position male connector, an antenna and other components for wireless data transmission. The components on the top and bottom PCB communicate through the two connectors. **b**–**c**, **In vitro characterization of the device for miniaturized wireless sensing of NO and ROS with cell-based biosensors**. Wireless signal over time from the NO (b) and ROS (c) sensors encapsulated in the device and immersed in bacterial growth media supplemented with 5 mM and 20 mM, respectively. Low-power CMOS-integrated photodiodes converted bioluminescence emitted from the bacterial sensor into a photocurrent, which was converted into quantifiable digital data and transmitted wirelessly to the external device. Lines represent the mean, and error bars denote the SEM for three independent replicates, conducted with one induced device (NO or ROS) and one uninduced device (Buffer); Rel. photocurrent, Relative Photocurrent.

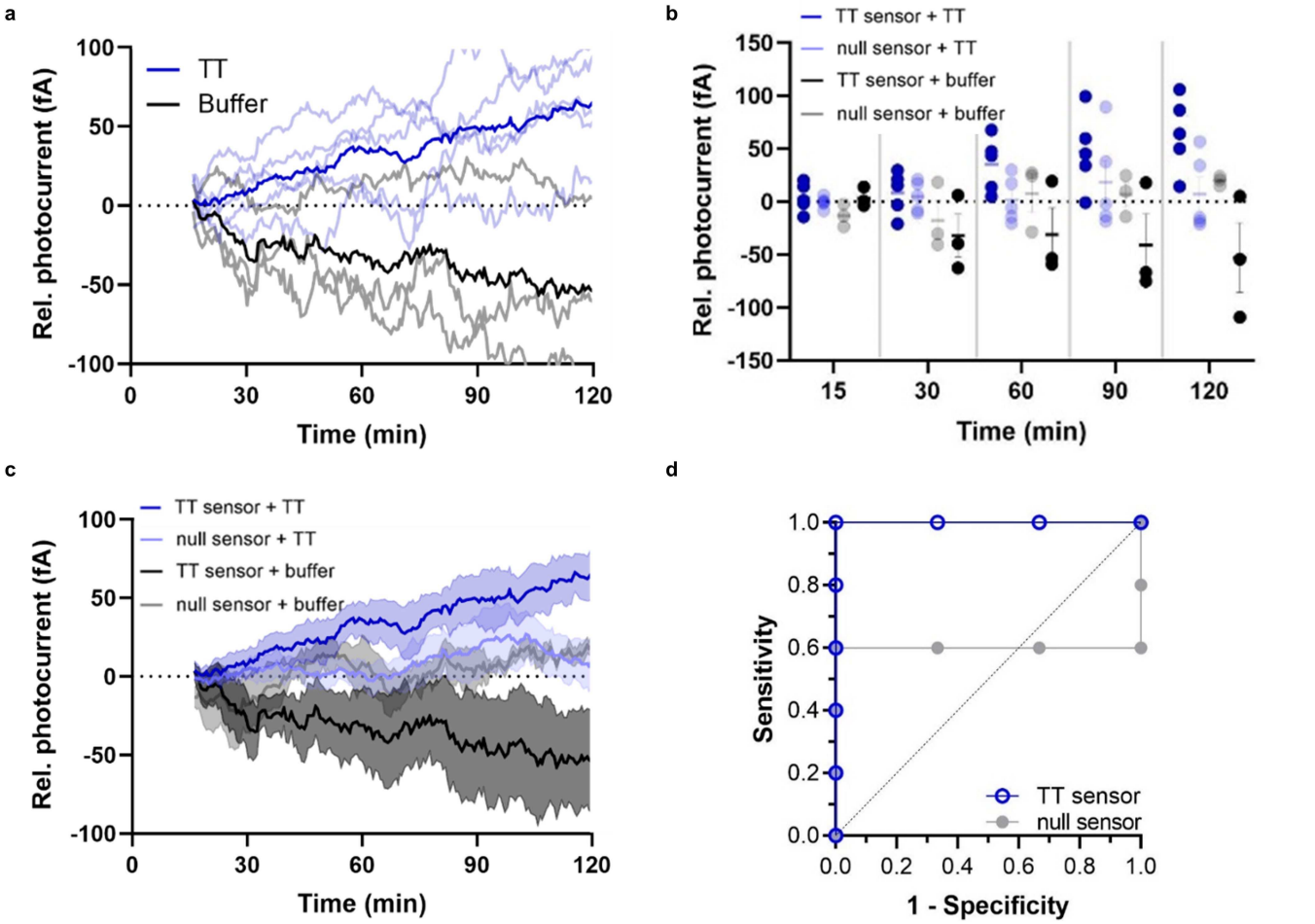

Extended Data Fig. 10 | In vivo validation of the integrated bacterial-electronic pill. a,**b**, Individual replicates of TT sensing in the pig intestinal environment. The devices with the TT sensor were deposited in the intestinal compartments and TT (100 mM, blue) or buffer alone (black) were injected after temperature stabilization (~15 min, 37 °C). Readings from the device were wirelessly collected for 120 min following device deposition. Dark trace represents the mean of 3 replicates measurements (3 animals on different days, 2 devices per pig, in two different compartments) and pale traces indicate the individual current values for a given device (two channels measured per device). Photocurrents are provided relative to a one-time calibration value at t = 15 min. Non-induced sensor cells (black lines) decrease their luminescence output throughout the experiment (as shown in vitro, tested in simulated intestinal fluid, Extended Data Fig. 8b), while induced cells express higher levels of luciferase, compensating signal loss over time. For all the replicates, the response of the device placed in the compartment with TT was clearly distinguishable from that of the device in the compartment with the buffer control. **b**, For clarity, individual photocurrent values corresponding to different time points (15, 30, 60 and 120 min) for n = 3 or n = 5 samples for different set of conditions, including: TT sensor + TT, null sensor + TT, null sensor + buffer and TT sensor + buffer. Data are represented as mean ± SEM. **c**, **Comparison of light detection between different chambers**. E. coli Nissle strains containing a functional biosensor circuit for TT detection (TT sensor), and E coli Nissle without the gene for luciferase (null sensor) were loaded into the device. Devices were deposited in the intestine compartments and after temperature stabilization (~15 min), TT (100 mM, blue) or buffer alone (black) were injected. Compartmentalized intestines were kept inside the abdomen, at 37 °C, and wireless signals transmitted from inside the abdomen were collected for 120 min to analyze the kinetic response of the devices in the abdominal cavity of the pig. Photocurrents provided relative to a one-time calibration value at t = 15 min. Non-induced sensor cells (black lines) decrease their luminescence output throughout the experiment (as shown when tested in simulated intestinal fluid, Extended Data Fig. 8b), while induced cells express higher levels of luciferase compensating signal loss over time. The response of the device placed in the compartment with TT was clearly distinguishable from that of the device in the compartment with the buffer control. Null cells (light blue and grey traces) maintain constant values throughout. Error bars denote SEM for three experiments (3 animals on different days, 2 capsules per animal). **d**, **Validation of the whole integrated device for miniaturized wireless biosensing in living pigs over time**. The receiver operating characteristic (ROC) of the device sensing TT reached a sensitivity and specificity of 100% at 120 min.

nature portfolio

Corresponding author(s): Traverso G, Yazicigil RT, Lu TK

Last updated by author(s): Jan 20, 2023

Reporting Summary

Nature Portfolio wishes to improve the reproducibility of the work that we publish. This form provides structure for consistency and transparency in reporting. For further information on Nature Portfolio policies, see our Editorial Policies and the Editorial Policy Checklist.

Statistics

For all statistical analyses, confirm that the following items are present in the figure legend, table legend, main text, or Methods section.

n/a	Confirmed
☐	☒ The exact sample size (*n*) for each experimental group/condition, given as a discrete number and unit of measurement
☐	☒ A statement on whether measurements were taken from distinct samples or whether the same sample was measured repeatedly
☐	☒ The statistical test(s) used AND whether they are one- or two-sided *Only common tests should be described solely by name; describe more complex techniques in the Methods section.*
☒	☐ A description of all covariates tested
☐	☒ A description of any assumptions or corrections, such as tests of normality and adjustment for multiple comparisons
☐	☒ A full description of the statistical parameters including central tendency (e.g. means) or other basic estimates (e.g. regression coefficient) AND variation (e.g. standard deviation) or associated estimates of uncertainty (e.g. confidence intervals)
☐	☒ For null hypothesis testing, the test statistic (e.g. *F*, *t*, *r*) with confidence intervals, effect sizes, degrees of freedom and *P* value noted *Give P values as exact values whenever suitable.*
☒	☐ For Bayesian analysis, information on the choice of priors and Markov chain Monte Carlo settings
☒	☐ For hierarchical and complex designs, identification of the appropriate level for tests and full reporting of outcomes
☒	☐ Estimates of effect sizes (e.g. Cohen's *d*, Pearson's *r*), indicating how they were calculated

Our web collection on statistics for biologists contains articles on many of the points above.

Software and code

Policy information about availability of computer code

Data collection	We used Cadence IC 6.1.7 for circuit design, layout design, and simulations (https://www.cadence.com/en_US/home.html) and Calibre 2016 for circuit verification (https://eda.sw.siemens.com/en-US/ic/calibre-design/circuit-verification/). Luminescence signal in the chambers were quantified using FIJI (ImageJ).
Data analysis	GraphPad Prism version 9.1.2 (Graph Software, San Diego, 524 CA, USA, http://www.graphpad.com). Sequences were analyzed using SnapGene version 5.1.2 (www.snapgene.com). BD FACSDiva 9.0 and FlowJo software v10 were used to export and process flow cytometry software files and analyze data and stadistics.

For manuscripts utilizing custom algorithms or software that are central to the research but not yet described in published literature, software must be made available to editors and reviewers. We strongly encourage code deposition in a community repository (e.g. GitHub). See the Nature Portfolio guidelines for submitting code & software for further information.

Data

Policy information about availability of data

All manuscripts must include a data availability statement. This statement should provide the following information, where applicable:

- Accession codes, unique identifiers, or web links for publicly available datasets
- A description of any restrictions on data availability
- For clinical datasets or third party data, please ensure that the statement adheres to our policy

All data are provided in the paper and in Supplementary Material, genetic parts and plasmids will be available from Addgene upon publication. Correspondence and and requests for further materials should be addressed to GT, RTY and TKL.

Human research participants

Policy information about studies involving human research participants and Sex and Gender in Research.

Reporting on sex and gender	N/A
Population characteristics	N/A
Recruitment	N/A
Ethics oversight	N/A

Note that full information on the approval of the study protocol must also be provided in the manuscript.

Field-specific reporting

Please select the one below that is the best fit for your research. If you are not sure, read the appropriate sections before making your selection.

☒ Life sciences ☐ Behavioural & social sciences ☐ Ecological, evolutionary & environmental sciences

For a reference copy of the document with all sections, see nature.com/documents/nr-reporting-summary-flat.pdf

Life sciences study design

All studies must disclose on these points even when the disclosure is negative.

Sample size	Sample sizes for all in vitro measurements were selected at n=3 to provide a sufficient sampling of the performance of the sensors, based on previous studies from Rubens, J. R, Nat. Commun. 7, 1–10 (2016). For mice experiments, n=5, this sample size was chosen based on previous studies (Riglar, D. T. et al. Nat. Biotechnol. 35, 653–658 (2017)). For swine experiments n=3, 4 or 5 as reported in the figure captions. A sample size of 3-5 individuals was chosen based on previous results showing that this group size is sufficient to power analysis of changes in the kinetics of a dosed small molecule drug, which was expected to have a smaller effect size than the sensor validation experiments in the present work. (Kirtane, A. R. et al. Nature Communications 9, 2 (2018).2., Kirtane, A. R. et al. Science Translational Medicine 11, (2019)). For in vitro viability experiments, a power analysis (alpha = 0.05, beta = 0.2) gave a samples size of 4, for a worst-case SD = 0.5 log-units and a minimum effect size of 1 log-unit. N was chosen to be larger than this value. All individual data points are shown in figures, and total size spanning all independent experiments is reported in the figure captions.
Data exclusions	No data was excluded from analysis.
Replication	All experiments were performed at least three times (independent biological triplicates) by at least one co-authors. All attempts at replication were successful.
Randomization	For mouse experiments, animals were randomly allocated to experimental groups. Pigs were also randomly selected for the experiments and housed under conventional conditions.
Blinding	Blinding is not relevant to our study. The data presented are quantitative values (obtained as described in Methods) and did not require subjective judgment or interpretation.

Reporting for specific materials, systems and methods

We require information from authors about some types of materials, experimental systems and methods used in many studies. Here, indicate whether each material, system or method listed is relevant to your study. If you are not sure if a list item applies to your research, read the appropriate section before selecting a response.

Materials & experimental systems

n/a	Involved in the study
☒	☐ Antibodies
☒	☐ Eukaryotic cell lines
☒	☐ Palaeontology and archaeology
☐	☒ Animals and other organisms
☒	☐ Clinical data
☒	☐ Dual use research of concern

Methods

n/a	Involved in the study
☒	☐ ChIP-seq
☐	☒ Flow cytometry
☒	☐ MRI-based neuroimaging

Animals and other research organisms

Policy information about studies involving animals; ARRIVE guidelines recommended for reporting animal research, and Sex and Gender in Research

Laboratory animals	Male C57BL/6J mice (8-10 weeks of age) were obtained from Jackson Labs (Stock No: 000664). Female Yorkshire pigs (50-95kg, 6-7 months at time of experiment, terminal), were received from Cummings Veterinary School at Tufts University in Grafton, MA.
Wild animals	The study did not involved wild animals.
Reporting on sex	For pig experiments, female pigs were used. We use predominantly female swine because they are more amenable to being socially housed and tend to be less aggressive. For mouse experiments all male mice were used because specific effects have been documented for dextran sodium sulfate (DSS) colitis in female mice that partially protect against chemically induced colitis, though this is still an area of ongoing research. In our study, the data presented in mice validates the functionality of the bacterial sensors in vivo; potential sex-specific effects in the mouse model are not relevant to the conclusions presented in this study.
Field-collected samples	The study did not involve samples collected from the field.
Ethics oversight	Approval for mouse and pig experiments was obtained from the Committee on Animal Care at the Massachusetts Institute of Technology.

Note that full information on the approval of the study protocol must also be provided in the manuscript.

Flow Cytometry

Plots

Confirm that:

☒ The axis labels state the marker and fluorochrome used (e.g. CD4-FITC).

☒ The axis scales are clearly visible. Include numbers along axes only for bottom left plot of group (a 'group' is an analysis of identical markers).

☒ All plots are contour plots with outliers or pseudocolor plots.

☒ A numerical value for number of cells or percentage (with statistics) is provided.

Methodology

Sample preparation	For flow cytometry, cells were diluted in cold 1x PBS and 2% sucrose to reach an optical 360 density of 0.02 (at 600 nm), then assayed on a BD LSRFortessa.
Instrument	BD LSRFortessa HTS1
Software	FlowJo software v10, BD FACSDiva 9.0
Cell population abundance	No sorting was performed for this study
Gating strategy	A minimum of 10,000 gated events was recorded. Forward scatter (FSC) and side scatter (SSC) were used to gate for cells excluding debris. The GFP emission was collected using the FITC detector with a 530/30 filter. Side scatter pulse height (SSC-H) was used to threshold on cells. Doublet gating was done on a SSC-W vs SSC-H plot, side scatter pulse width (SSC-W).

☒ Tick this box to confirm that a figure exemplifying the gating strategy is provided in the Supplementary Information.